

Quantum Spin Hall Materials

Chuanwu Cao and Jian-Hao Chen*

The quantum spin Hall (QSH) effect describes the state of matter in certain 2D electron systems, in which an insulating bulk state arises together with helical states at the edge of the sample. In stark contrast to its closest kin, the integer quantum Hall state, the QSH state exists only in time-reversal symmetric system (e.g., in non-magnetic materials and without the application of external magnetic field). This article reviews the development of the understanding and construction of the QSH states after their first theoretical proposal, with an emphasis on the materials perspective. Certain semiconductor quantum wells and 2D materials with strong spin-orbit coupling have been found to support QSH states.

1. Introduction

The quantum Hall (QH) state, discovered in 1980,^[1] gave an example of dramatic modifications to the electronic dispersion relation in 2D systems by the application of high magnetic field. In the QH state, the bulk of the 2D electron system is insulating and the edges are conducting with the dissipationless channels called the chiral edge states. **Figure 1a** is a sketch of the QH states of matter with such edge states. For the top edge, for example, the electrons can only propagate to the right (defined as propagating “forward” in the rest of the text) while for the other edge, the electrons can only propagate to the left (defined as propagating “backward” in the rest of the text). In other words, electrons are spatially separated into two different lanes located at the two edges of the sample, with different directions of their movement. Due to such separation in real space, in sufficiently large sample where the overlap between two edge states is negligible, backscattering of the electrons along the edges is forbidden, as there are simply no counter-propagating modes that are physically presented near any of the chiral modes. Such separation is achieved with two preconditions: 1) the existence of the chiral edge states, 2) an insulating bulk. These conditions can be achieved in ultrahigh mobility 2D electron systems under high magnetic field at sufficiently low temperature. Examples of such ultrahigh mobility 2D electron systems are 2D electron gas at the interface


of semiconductors^[2] or insulators,^[3,4] and charge carriers in 2D materials, such as graphene,^[5] black phosphorus,^[6] InSe,^[7] and certain semiconducting transition metal dichalcogenides.^[8,9] Recently, certain thin films of 3D materials with high mobility also exhibit QH effect.^[10–12] Although such dissipationless edge states itself is highly desirable in electronic circuits, the general requirement of strong magnetic field and low temperature limits its practical applications.

Can one realize a state of matter with insulating bulk and highly conductive edge states, without applying a magnetic field? The quantum spin Hall (QSH) state,^[13–17] predicted by Kane, Mele, and Zhang,^[18–21] is exactly such a state of matter promised to have the above-mentioned properties. A simplified schematic of a system in a QSH state is shown in **Figure 1b**. An example of QSH band structure is shown in **Figure 2**. Comparing with QH states, the edge states in a QSH insulator is spin-polarized. Take **Figure 1b** as an example, the top edge contains one spin-up mode propagating forward and one spin-down mode propagating backward; conversely, the bottom edge contains one spin-down mode propagating forward and one spin-up mode propagating backward. Due to the fact that the spin of the electrons/holes in these modes is locked with its velocity, or the direction of propagation, such configuration of electronic modes is called the “helical edge states.” Such helical edge states have a net transport of spin forward along the top edge and a net transport of spin backward along the bottom edge, just like a net transport of charge in the QH states. Both the QH states and the QSH states are topological states of matter. Different from the chiral edge states in QH systems, the helical edge states in QSH systems are protected under time-reversal (TR) symmetry, thus backscattering by nonmagnetic impurities is forbidden. Furthermore, such edge states are robust against the geometry disorder of the sample edges and other perturbation effects,^[18,22] which is topologically protected and described by Z_2 invariant.^[18,23] Thus, the QSH state of matter is also called 2D topological insulator. Even though TR symmetry could be broken by fluctuations or the existence of magnetic impurities, such TR symmetry protected edge states could provide a route to quantum electronic devices with low dissipation.

The absence of backscattering in QH edge states can be understood as there is no opposite moving state in one edge. Although a QSH edge contains both forward and backward moving states, backscattering under TR symmetry is also forbidden. Such effect can be compared to the so-called “antireflection coating”. **Figure 3a,b** show two scattering paths of an electron in a QSH edge. In both scattering paths, the electron is scattered from the forward moving edge state to the backward moving state by a non-magnetic impurity. Since these two paths are TR counterparts,

C. Cao, Prof. J.-H. Chen
International Center for Quantum Materials
School of Physics
Peking University
No. 5 Yiheyuan Road, Beijing 100871, China
E-mail: chenjianhao@pku.edu.cn

Prof. J.-H. Chen
Beijing Academy of Quantum Information Sciences
Beijing 100193, P. R. China

 The ORCID identification number(s) for the author(s) of this article can be found under <https://doi.org/10.1002/qute.201900026>

DOI: 10.1002/qute.201900026

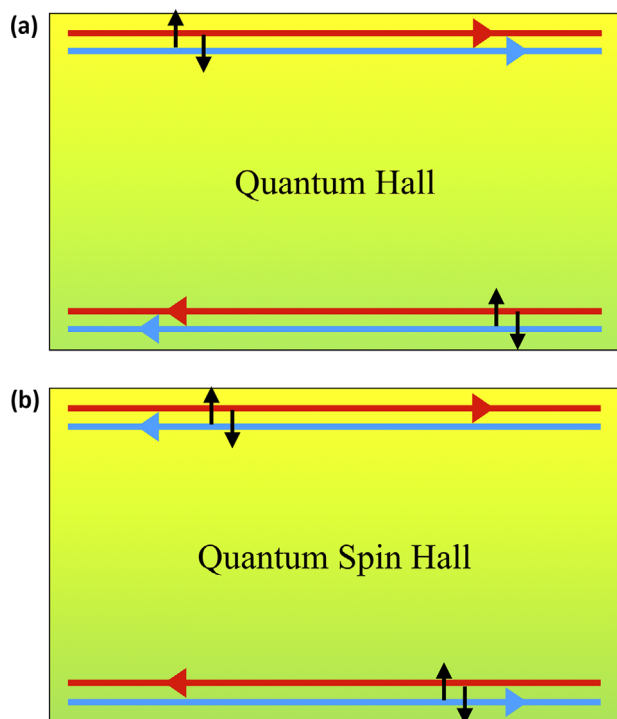


Figure 1. Sketches of quantum Hall edge states and quantum spin Hall edge states. Red and blue lines are edge states. Arrows along the lines indicate carriers' moving direction in such edge states. a) In quantum Hall state, the bulk is insulating and the edge states are chiral. The top edge contains only forward moving states and the bottom edge contains only backward moving states. b) In quantum spin Hall state, the bulk is insulating and the edge states are helical. Each edge contains both forward moving and backward moving edge states with different spin (Kramers pairs, actually).

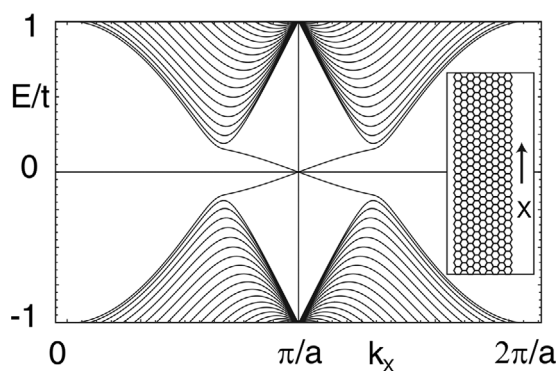


Figure 2. 1D energy bands for a strip of graphene. The gap is opened by spin-orbit coupling. The bands crossing the gap are spin filtered edge states. Inset: a strip of graphene. Reproduced with permission.^[19] Copyright 2005, APS.

under TR symmetry, the electron wavefunctions after moving along these two scattering paths are differed with a phase of 180° and interfere destructively.^[13] In close analogy with antireflection coating in optics, the backscattered electron wavefunctions in the QSH edge states are expected to be completely canceled, which leads to the perfect transmission of electrons at the presence of nonmagnetic impurities. If the TR symmetry is broken,



Chuanwu Cao received his bachelor of physics degree in 2014 and is working as a Ph.D. candidate at Peking University, China. He has experience in nanoelectronics and in situ quantum transport. In his Ph.D. program, he developed an in situ transport measurement system and studied in situ modified graphene. Recently, he is studying quantum spin Hall materials using the in situ

quantum transport measurement system.



Jian-Hao Chen obtained his Ph.D. in physics at University of Maryland, USA (2009). Thereafter, he worked as a research fellow at University of Maryland (2009–2011) and University of California at Berkeley (2011–2013). Since 2013, he has been associate professor and principle investigator of the Laboratory for Nanoelectronics and in-situ Quantum Transport at the School of Physics, Peking

University, Beijing, China. His present research is focused on studying the physics and applications of low-dimensional electronic materials and heterostructures, manipulation of material properties at the atomic scale, and in-situ quantum transport characterization in ultrahigh vacuum environment.

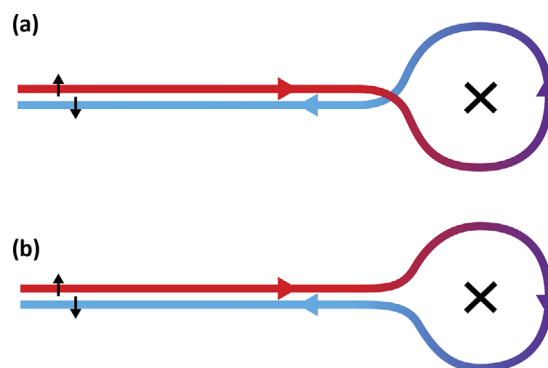


Figure 3. Sketches of scattering process of quantum spin Hall edge states. A quantum spin Hall edge state can be scattered into its counterpart in two directions by a nonmagnetic impurity (black cross), shown in (a) and (b). The two paths are time-reversal counterparts and they interfere destructively. As a result, backscatterings in quantum spin Hall edges are forbidden.

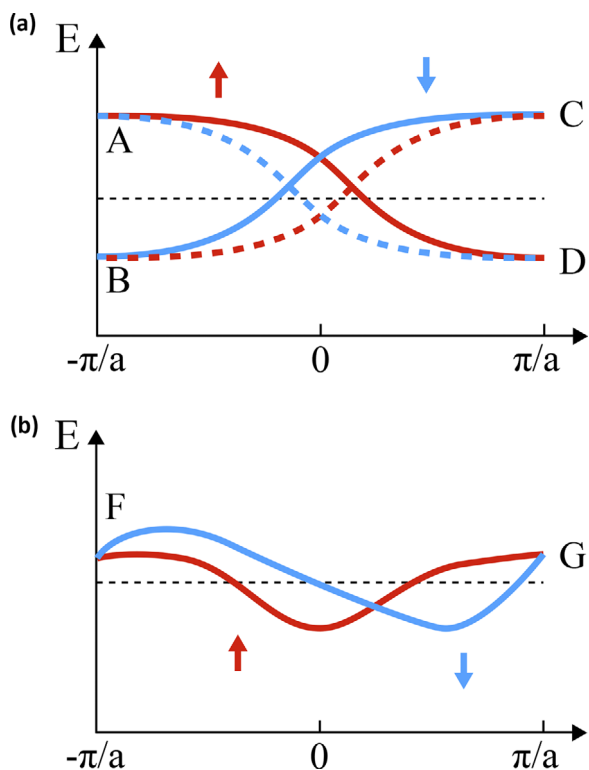


Figure 4. Sketches of 1D band structure. Schematic band structure in a) quantum spin Hall edges and b) 1D spinful system. (a) Solid lines and dash lines represent the top edge and the bottom edge, respectively. For a single edge, only one Kramers doublet appear at a given Fermi surface. (b) Even numbers of Kramers doublets appear at a given Fermi surface except at the extremum points.

such as under a magnetic field or if the impurity carries a magnetic moment, these two scattering paths are no longer linked by TR symmetry. Thus, the two scattered wavefunctions cannot interfere destructively and backscattering is no longer forbidden. It is worthwhile to point out that there are helical edge states with broken TR symmetry that are also coined “QSH states.”^[24,25] These “QSH states” are protected by other symmetries (such as U(1) symmetry of spin rotations,^[24] combined symmetry of TR and primitive-lattice-translation^[25], etc.) instead of solely the TR symmetry. The protection mechanisms in these “QSH states” are similar to the previously mentioned “antireflection coating.” As the two scattering paths are linked by an inversion under the protection symmetry, the backscattering wavefunction will interfere destructively and the helical edge states are protected.

Edge states in a QSH system cannot be realized in 1D systems. **Figure 4** is a sketch of the dispersion relation of QSH edges (Figure 4a) and that of a spinful 1D system (Figure 4b). Because the dispersion relation of any single state will need to be degenerate at the two boundaries of the first Brillouin zone, a forward moving channel always has a backward moving counterpart with the same spin at any given Fermi surface. In QSH systems, such counterpart is located at the other edge of the sample, thus the protection against backscattering for nonmagnetic impurities is somewhat similar to the exponential protection seen in Majorana modes at the two ends of a semiconductor

nanowire-superconductor heterostructure.^[26] Comparing with a spinful 1D electron system, QSH edge states can be regarded as separating this 1D system into top and bottom edges of a 2D system. Take Figure 4a as an example, if one follows the dispersion relation marked by the solid red line from point A to point D (the spin-up state at the top edge of the sample), the state did not get back to the same energy (e.g., $E_A \neq E_D$). The degeneracy of point A and point D is fulfilled by the QSH states at the other edge, which has a dispersion relation from point C to point B (red dashed line in Figure 4a, $E_A = E_C$ and $E_B = E_D$). Similarly, for the spin-down state at the top edge, which is shown as the blue solid line in Figure 4a, the degeneracy of this state at the boundary of the first Brillouin zone is fulfilled together with the spin-down state at the bottom edge (blue dashed line in Figure 4a). The concept and picture in QSH effect can be generalized to a 3D electron system, which is called (3D) topological insulator, for which each surface contains half of the 2D Dirac fermions in the material and the 3D bulk is insulating. It is firstly proposed^[27] and observed^[28] in $\text{Bi}_{1-x}\text{Sb}_x$.

It is worthwhile to point out that “spin-up” and “spin-down” in QSH system is equivalent as calling it the “forward moving state at one edge” and “backward moving state at the same edge.” This is because QSH effect is originated from strong spin-orbit coupling^[19,20] and spin is no longer a good quantum number in this case. What “spin-up/spin-down” really means is that the helical edge states form Kramers pairs, and the band crossing point for one edge in Figure 4a is called the Kramers point. Kramers theorem points out that in a TR symmetric system with half-integer total spin, each energy level is at least doubly degenerated.^[29] In QSH system, the double degeneracy represents forward moving and backward moving edge states.

Besides dissipationless electron channels, QSH effect attracts great interest because it also provides solutions for quantum computing. It is proposed that quantum computing can be realized by Majorana bound states.^[30] A QSH insulator coupled with a superconductor as a Josephson junction has predicted to exhibit a fractional Josephson effect, which is related to Majorana fermions.^[31] Moreover, a QSH edge coupled with magnet/superconductor/magnet heterostructure is proposed to be able to probe the Majorana bound states inside the heterostructure.^[32] Fractional QSH effect^[33] is also predicted to host Majorana bound states,^[34–36] providing another way to realize states for topological quantum computing.

2. Quantum Spin Hall Effect in Quantum Wells

QSH effect was firstly proposed in graphene.^[19] Unfortunately, due to the combined effect, that carbon has a small spin-orbit coupling strength and the arrangement of the carbon atoms in the planar honeycomb structure eliminates the spin-orbit coupling effect to the first order, the overall spin-orbit coupling of graphene is extremely small.^[37,38] Calculations show that spin-orbit coupling in graphene can open a gap at the Dirac point by as much as 10^{-3} meV, which require a very low temperature of $T \ll 10$ mK to observe QSH effect,^[38] which is beyond the reach of conventional cryogenic technology in solid state physics.

QSH effect was also independently proposed in semiconductors with strain gradients^[20] or inverted band structures.^[21] The

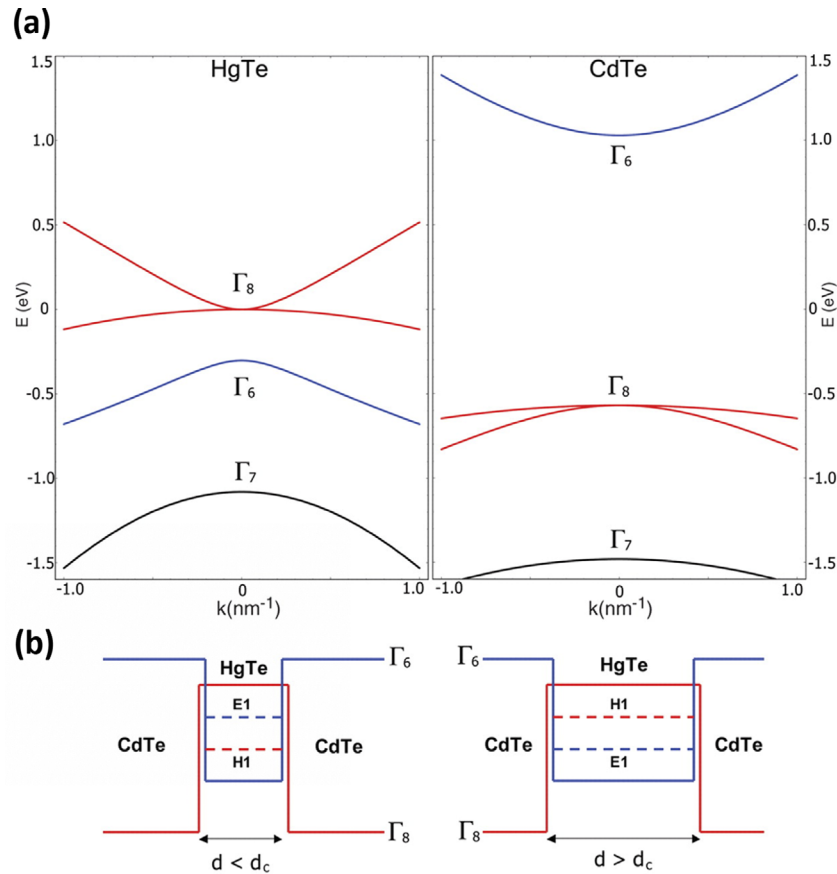


Figure 5. Band structures of bulk HgTe, CdTe, and HgTe quantum wells. a) Bulk energy bands of HgTe and CdTe near the Γ point. b) The CdTe-HgTe-CdTe quantum well in the normal regime ($d < d_c$) and inverted regime ($d > d_c$). Dash lines are quantum well subbands. In normal regime, Γ_6 subband E_1 is higher than Γ_8 subband H_1 , which is the same as bulk CdTe. In inverted regime, Γ_6 subband E_1 is lower than Γ_8 subband H_1 , which is inverted compared with bulk CdTe. Due to such band inversion, helical edge states appear in HgTe quantum well's band gap. Reproduced with permission.^[21] Copyright 2006, AAAS.

inverted band structure was realized in HgTe quantum wells^[39] and InAs/GaSb quantum wells.^[40] This section reviews the main experimental results in these two material systems. The study has also gone beyond 2D electronic systems and led to the discovery of 3D topological insulators,^[27,41] which is beyond the scope of this article.

2.1. HgTe Quantum Wells

QSH was firstly experimentally realized in HgTe quantum wells.^[39] Ref. [21] proposed a general way for searching QSH insulators and predicted HgTe quantum wells sandwiched by CdTe layers are QSH insulators when the thickness d of the HgTe layer is above a critical thickness d_c . In the barrier material CdTe, the important bands near the Fermi surface are an s-type Γ_6 conduction band and a p-type Γ_8 valence band. In the well material HgTe, the band structure is inverted due to spin-orbit coupling and the Γ_6 band is lying below the Γ_8 band. In the CdTe/HgTe/CdTe quantum well, when HgTe is thinner than a critical thickness $d_c = 6.3$ nm, CdTe dominates the behavior of the quantum well. In such case, the subbands of the HgTe quantum well would order like those in CdTe, which means that the Γ_6 subband is

lying above and the Γ_8 subband, as shown in the left panel of Figure 5b. On the other hand, when the thickness of the quantum well is greater than the critical thickness d_c , the influence of HgTe dominates and the subbands in the HgTe quantum well are inverted, which means that the Γ_6 subband becomes the valence band, as shown in the right panel of Figure 5b. In this condition, conducting states emerge at the bulk gap near the edge of the sample where different spins are locked with modes propagating in different directions and at different edges of the sample. Such conducting edge states are called helical edge states. However, the confinement energy of quantum wells will decrease when the thickness of the HgTe layer increases, and the unique properties of the HgTe quantum well will eventually disappear.^[15] Thus, QSH states were experimentally observed in samples with the width of the HgTe layer in the range of $d = 6.6$ to 8.5 nm.^[39,42–44] At the critical thickness $d_c = 6.3$ nm, the band gap of the HgTe quantum well vanishes and magnetoresistance measurements show that the carriers are massless Dirac fermions.^[45,46]

QSH effect was firstly demonstrated by transport measurement in HgTe quantum wells sandwiched by Hg_{0.3}Cd_{0.7}Te barriers.^[39] Devices were fabricated by molecular beam epitaxy and defined in Hall bar geometry. Figure 6a shows the transport results^[39] of HgTe quantum wells. Trace I is the longitudinal

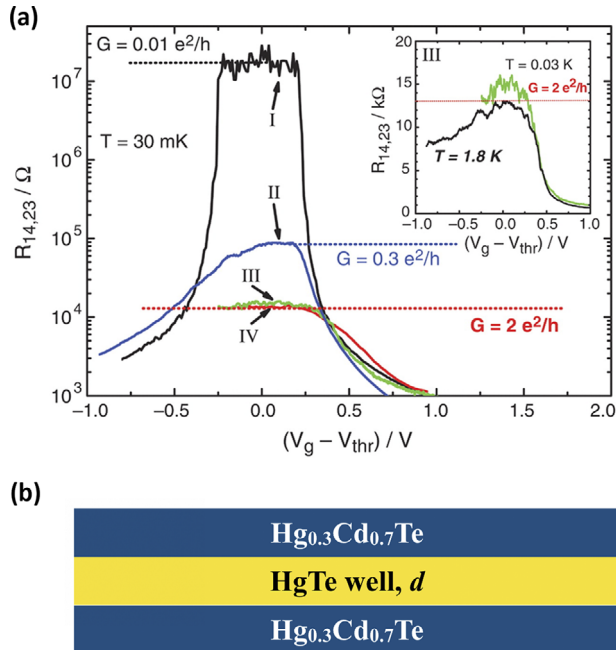


Figure 6. Resistance of HgTe quantum wells. a) The longitudinal four-terminal resistance of various quantum wells as a function of the gate voltage measured for $B = 0$ T at $T = 30$ mK. I): $d = 5.5$ nm, normal. II,III,IV): $d = 7.3$ nm, inverted. The device sizes are $(20.0 \times 13.3) \mu\text{m}^2$ for devices I and II, $(1.0 \times 1.0) \mu\text{m}^2$ for device III, and $(1.0 \times 0.5) \mu\text{m}^2$ for device IV. In normal regime (I), HgTe quantum wells show insulating behavior in the band gap. In inverted regime (II,III,IV), HgTe quantum wells are edge conducting while the bulk are insulating. When the distance between two electrodes is small enough to avoid the inelastic scatterings, break the helical edge states into sections (III,IV), measured resistances fit with the predicted value $R = 2e^2/h$. Such value is independent with sample's width and temperature in quantum spin Hall regime. Inset: resistance of two samples from the same wafer, having the same device size (III). b) HgTe quantum well structure in ref. [39]. Reproduced with permission.^[39] Copyright 2007, AAAS.

four-terminal resistance of a normal ($d < d_c$) quantum well. In the normal regime, subbands in the HgTe quantum wells are not inverted. When the Fermi surface is lying in the gap, the quantum well shows conventional insulating behavior, as trace I demonstrated. Traces II, III, and IV are resistance of inverted ($d > d_c$) quantum wells. In the inverted regime, when the Fermi level is in the gap, the bulk becomes insulating while the edges remain conducting due to the emergence of the QSH edge states. Thus, the resistance of the whole sample in the gap is dominated by the helical edge states and is significantly lower than the not-inverted one. By applying the Landauer–Büttiker formalism,^[47] the residual conductance in the QSH gap can be calculated.^[21,22,42] In general, a single edge channel has a conductance quanta of e^2/h . In the Hall bar four-terminal configuration, the residual conductance should be $G = 2e^2/h$ as there is one forward moving channel per edge. At the meantime, due to the edge conduction configuration, the residual conductance should be independent of the width of the samples unless the two edges are too close so that they couple together and destroy the QSH effect.^[48] Though QSH edge states are protected by TR symmetry and elastic backscattering is forbidden at the edges,

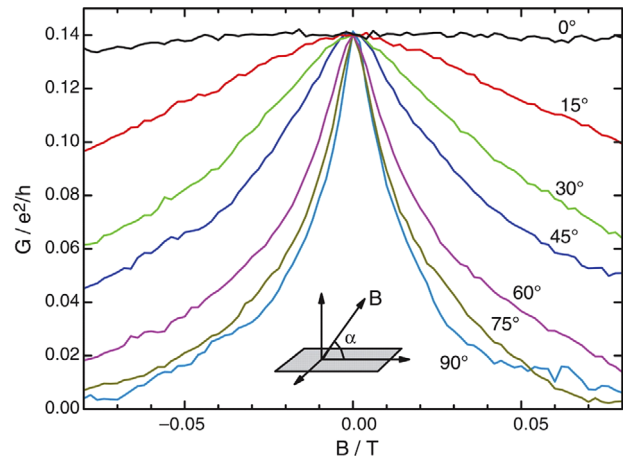


Figure 7. Magnetoconductance for HgTe quantum well in quantum spin Hall regime. Four-terminal magnetoconductance of HgTe quantum well in quantum spin Hall regime as a function of magnetic field and its tilt angle measured at $T = 1.4$ K. Device geometry: $(20 \times 13.3) \mu\text{m}^2$, $d = 7.3$ nm. As the magnetic field breaks the time-reversal symmetry, backscatterings are no longer forbidden and the edge conductance is suppressed. A strong anisotropy is shown. Reproduced with permission.^[39] Copyright 2007, AAAS.

inelastic scatterings will break the edge states to sections. Thus, predicted quantized residual conductance can only be observed in small Hall bars where continuous edge states survive in such a distance. Traces II, III, IV in Figure 6a come from different devices with different sizes. The size of device II is $20.0 \times 13.3 \mu\text{m}^2$, which is much larger than the inelastic mean free path in the device. As a consequence, the measured residual conductance is smaller than the predicted value $G = 2e^2/h$. Voltage probe distances in device III ($1.0 \times 1.0 \mu\text{m}^2$) and IV ($1.0 \times 0.5 \mu\text{m}^2$) are close enough to show the helical edge conductance to be near $2e^2/h$, which is strong evidence of the existence of the QSH states.

When applying a magnetic field to the sample, mixing between the two conduction channels at the same edge is nonzero and a Zeeman gap opens at the Kramers point of the edge states. In this situation, as the TR symmetry is broken, backscattering between the edge states is no longer forbidden, leading to a suppression of the residual conductance. **Figure 7** shows magnetoresistance data^[39] of the inverted HgTe quantum well in the gap. A sharp conductance peak is observed for perpendicular magnetic field. However, the residual conductance is less sensitive under a parallel magnetic field, which is originated from the fact that the Zeeman gap in a parallel magnetic field is two orders of magnitude smaller than that in a perpendicular magnetic field in the given sample.^[39]

It is worth noting that in the QSH regime, transport measurement results correlate strongly with measurement configurations. Take a multi-terminal device shown in the inset of **Figure 8**, for example,^[42] in a two-terminal resistance measurement configuration, $R_{14,14} = 3h/2e^2$ (here, $R_{14,14}$ means that current is injected between contacts 1 and 4, and voltage is measured between the same two contacts). Meanwhile, in a four-terminal resistance measurement configuration, $R_{14,23} = h/2e^2$ (here, $R_{14,23}$ means that current is injected between contacts 1 and 4, and

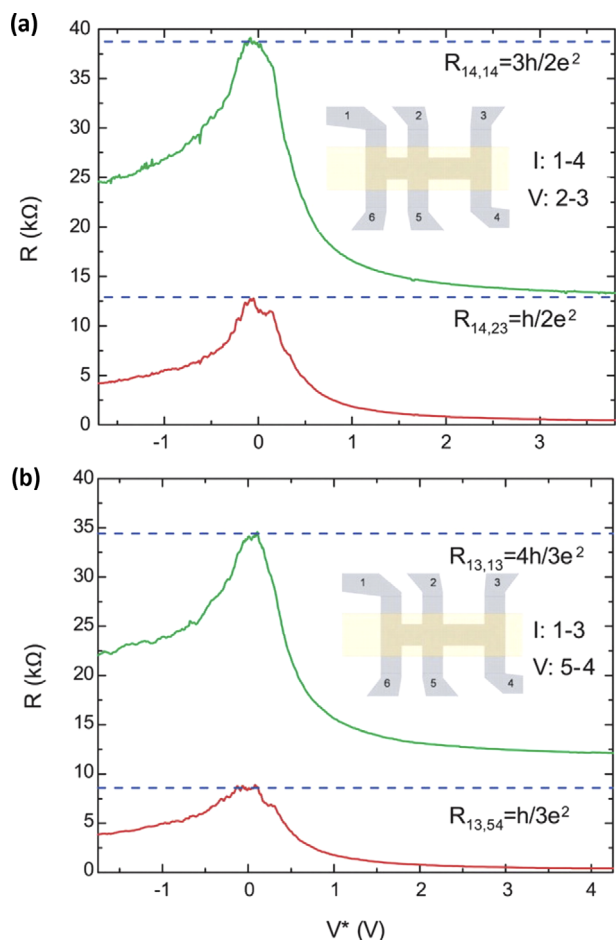


Figure 8. Nonlocal resistances of inverted HgTe quantum wells. Four- and two-terminal nonlocal resistance as a function of gate voltage in an HgTe Hall bar. The dash lines indicate the predicted resistance values in quantum spin Hall regime calculated by Landauer–Büttiker formalism. The insets show geometry of the devices and the measurements configurations. The yellow areas are gates. The nonlocal resistances fit well with the predictions, which is an unambiguous evidence of helical edge states. Reproduced with permission.^[42] Copyright 2009, AAAS.

voltage is measured between contacts 2 and 3).^[39,42] If one chooses to inject current and detect voltage at the same edge of the sample, in a two-terminal configuration, $R_{13,13} = 4h/3e^2$; while in a four-terminal configuration, $R_{13,54} = h/3e^2$. All the measurement results are consistent with the calculation of the Landauer–Büttiker formalism in a QSH system. These nonlocal results in different multiterminal geometries give an unambiguous evidence of the existence of the helical edge states.^[42]

Apart from the conventional resistance measurement, edge conduction can also be examined via transport measurements in the Josephson junction geometry.^[43] In general, a Josephson junction is characterized by measuring magnetic field B dependence of the critical supercurrent I_C . In ref. [43], a two-terminal Josephson junction composed by a rectangular HgTe quantum well located between two titanium/aluminum leads was fabricated. The dependence of I_C versus B of such device provides information for the distribution of supercurrent in the quantum well. When there is only edge conduction without bulk contribu-

tion, the I_C versus B curve has a sinusoidal double-slit pattern; when edge conduction coexists with some bulk conduction, a pronounced Fraunhofer interference peak shows up at the zero B field; when edge conduction is overwhelmed by bulk conduction, the I_C versus B curve completely recovers the Fraunhofer interference pattern. Edge conduction can also be examined by imaging current distribution directly using a scanning superconducting quantum interference device (SQUID) with $\approx 3 \mu\text{m}$ spatial resolution, which reports a regime that edge channel coexists with a conducting bulk.^[44]

2.2. InAs/GaSb Quantum Wells

To observe the QSH effect in HgTe quantum wells, precise growth control in the MBE process is required, and the device fabrication process is also highly challenging, as a result of the high volatility of Hg. Furthermore, HgTe is not a conventional quantum well material and only a few research groups can grow it. Such material issues have prevented fast development of the fundamental understanding and application of QSH states in HgTe quantum wells.

InAs/GaSb quantum wells, on the other hand, are more conventional and were also predicted to be QSH insulators shortly after the prediction of QSH states in HgTe quantum wells.^[49] The p -like valence band edge of GaSb is higher than the s -like conducting band edge of InAs, which provides the mechanism for man-made band inversion, in contrast to the heavy reliance on spin–orbit coupling in HgTe quantum wells. As can be seen in Figure 9a, in this new recipe, the electron subband and hole subband are separated in two layers. Electron subband in InAs (E_1) and hole subband in GaSb (H_1) can be shifted by changing the thickness of the quantum well, giving people more control over the electronic system. In certain range of thickness, the band edge of E_1 is lower than band edge of H_1 , which is called the inverted regime of the InAs/GaSb quantum wells. In such inverted regime, when moving away from the band edge (e.g., at finite k), the energy of E_1 and H_1 will cross at some point. The mixing between these two subbands at the degenerate points opens a hybridization gap E_g , which constitutes the bulk gap of the QSH insulator (see Figure 9b). The topological nature of InAs/GaSb quantum wells is more sensitive to the thickness of InAs layer d_2 , as shown in Figure 9c. As an example, GaSb layer thickness is set to $d_1 = 10 \text{ nm}$. The quantum well will be a normal insulator when $d_2 < 9 \text{ nm}$ and a QSH insulator when $d_2 > 9 \text{ nm}$. Switching on and off the QSH states by gate voltage was also proposed in InAs/GaSb quantum wells devices, as shown in Figure 9d. Here, “OFF” in such devices means that the insulating gap is topologically trivial and the Fermi level lies inside the gap. On the other hand, “ON” means that the Fermi level lies inside a topologically nontrivial gap and carriers move along the QSH dissipationless edges.

Unfortunately, studies show that in inverted InAs/GaSb quantum wells, the bulk remain conducting at milli-Kelvin temperatures^[50,51] though the predicted QSH gap is large enough for QSH effect to be observed in such temperatures.^[49] Nonetheless, various attempts were made to obtain experimental evidence for the existence of the helical edge states in InAs/GaSb quantum wells among the signal of a mildly conducting bulk. In ref. [51],

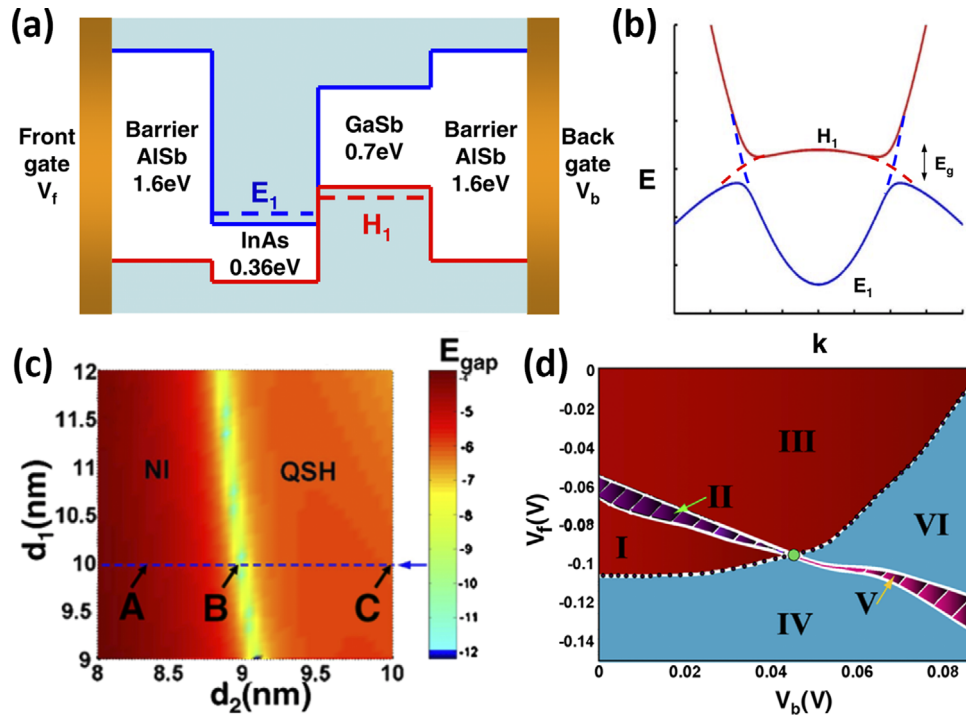


Figure 9. Theoretical predictions of InAs/GaSb quantum well. a) Band gap diagram for InAs/GaSb quantum well with AlSb barriers. The solid lines are bulk band edges and the dash lines are InAs/GaSb quantum well subbands. The E_1 subband is localized in the InAs layer and the H_1 subband is localized in the GaSb layer. b) Schematic band structure diagram. Hybridization between E_1 and H_1 opens the gap E_g . c) The energy gap E_g variation in d_1 - d_2 plane, where d_1 and d_2 are the thickness of GaSb layer and InAs layer, respectively. NI (normal insulator) and QSH (quantum spin Hall) denote the phase in the corresponding region. In the NI region, subband E_1 is higher than H_1 . In the QSH region, the band edge of E_1 sinks below that of H_1 where the band is inverted. d) Phase diagram of InAs/GaSb quantum well ($d_1 = d_2 = 10$ nm, barrier thickness = 30 nm) for different front and back gate voltages. Regions I, II, III are in the inverted regime and IV, V, VI are in the normal regime. In regions II and V, the Fermi surface is in the bulk gap. By applying gate voltages, the InAs/GaSb quantum wells can be tuned from region II to region V, which means turn “OFF” the quantum spin Hall edge states. Reproduced with permission.^[49] Copyright 2008, APS.

resistance in the inverted gap as a function of sample length and width is measured. The measured resistance is a parallel combination of bulk resistance and edge resistance. Bulk resistance can be estimated by measuring long QSH samples. By subtracting the estimated bulk conductance, a clear value of quantized conductance is shown. In ref. [52], using superconducting electrodes, Andreev conductance peaks that are consistent with Andreev reflection of the helical edge states are observed. Nonlocal measurements^[53,54] of InAs/GaSb quantum wells also give evidence for the existence of edge conduction channels.

In order to enable direct measurement of quantized conductance plateaus of the QSH edge states without the need to do background subtractions, one obvious way is, of course, to enhance the hybridization gap E_g ; a subtler method is to create a transport gap through interaction effects or through localization of the bulk conduction electrons. We shall review experimental attempts in both directions.

Changing the thickness of the InAs layer can tune the position of the subband in the quantum well. During this tuning, the quantum well changes from conventional insulator to shallowly inverted insulator, then deeply inverted insulator.^[53,55] The hybridization gap and observe a gap resistance close to $h/2e^2$.^[53] Ref. [56] reported a suppression of bulk conductance in InAs/GaSb quantum wells using dual-gate configuration. With a more insulating bulk, single edge resistance h/e^2 is observed.

Ref. [40] reported the realization of QSH conductance plateau using the second method: the authors use Si to dope the interface between GaSb and InAs during the MBE growth (see Figure 10a). The Si dopants act as impurities and localize the conducting bulk states at sufficiently low temperature, making the bulk truly insulating so that the edges are the only conducting channels. The nonmagnetic Si dopants have little effects on the QSH edge states because of the topological protection. Figure 10b shows quantized conductance plateaus in such devices. The quantization is better than other reported QSH conductance plateaus, giving a strong direct evidence of the existence of the helical edge states and indicating a good topological protection of such states. Note that there are two gaps in such samples: Si-doping-induced localization gap and hybridization-induced gap (QSH gap). Direct imaging of current distribution in Si-doped InAs/GaSb quantum wells confirms the existence of an insulating bulk and conducting edges.^[57]

Temperature-dependent resistance measurements show localization behavior at low temperature while the QSH gap is revealed at relatively higher temperature. When nonzero magnetic field is applied, however, the expected suppression (see Section 2.1) of the QSH conductance plateau is not observed. Instead, the conductance plateaus in such devices increase when perpendicular magnetic field is applied, which is different from the behavior of HgTe quantum wells.^[39] Under in-plane magnetic

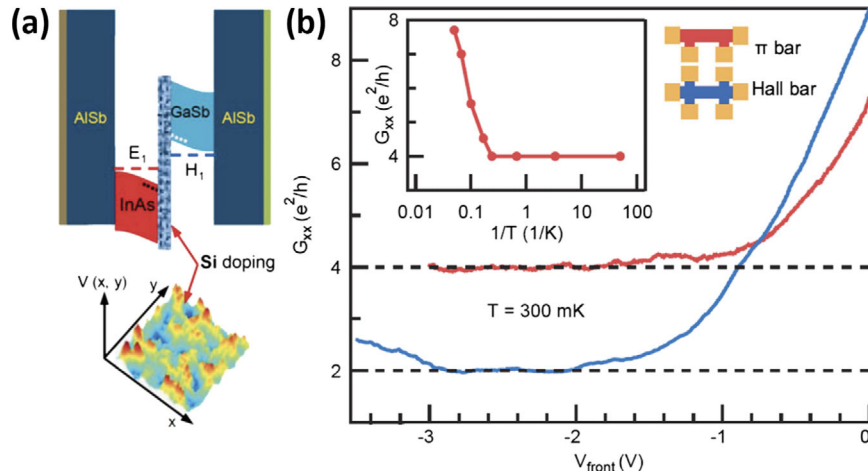


Figure 10. Conductance of Si doped InAs/GaSb quantum well in quantum spin Hall regime. a) Sketch of InAs/GaSb quantum well geometry and band structure. Si doped the interface between InAs and GaSb, make the bulk truly insulating at sufficient low temperature. b) Four-terminal conductance as a function of gate voltage. Wide conductance plateaus quantized to $2e^2/h$ and $4e^2/h$ are shown (for two different device configurations), indicating a strong topological protection of quantum spin Hall edge states. Inset: temperature dependence of conductance plateau values. The quantized value persists to 4 K. Reproduced with permission.^[40] Copyright 2015, APS.

field, the QSH conductance plateaus in such devices persist up to 12T, which challenges common understanding of the QSH effect. Ref. [58] used Ga source material with relatively low purity in the MBE process to reduce the conductivity of the bulk; however, the conductance quanta was not observed.

Ref. [55] reported the experimental effort along the first direction (e.g., enhancing the hybridization gap E_g) using strain engineering. In this work, strain was induced by alloying GaSb with InSb because their lattice constants are different. The strained quantum wells, InAs/Ga_{1-x}In_xSb, have larger hybridization gap compared with unstrained InAs/GaSb quantum wells. By measuring the temperature-dependent conductance of edgeless Corbino devices, the hybridization gap is fitted to be ≈ 250 K for the InAs/Ga_{0.68}In_{0.32}Sb quantum wells. The $h/2e^2$ resistance plateau in this system is shown in **Figure 11**. Such plateau was

observed in a $10 \times 5 \mu\text{m}^2$ Hall bar, significantly larger than other QSH devices.^[39,59] Under a perpendicular or in-plane magnetic field, the edge resistance increases in strained InAs/GaSb quantum wells, which is consistent with theoretical expectations.

As a side note, the helical edge states in Si doped InAs/GaSb quantum wells show behavior of strong interaction. In the strongly interacting regime, the correlated two-particle backscattering processes break the helical edge state into segments, which is called “helical Luttinger liquid.”^[60–62] Such processes reduce residual conductance from a temperature-independent quantized value to a power-law function of temperature, $G \propto T^\alpha$.^[62] Ref. [63] reports an exponent $\alpha \approx 0.32$ with a small excitation current $I = 0.1$ nA (see **Figure 12**). The quantized QSH conductance plateau will recover when applying a larger excitation current (or a larger bias voltage), as the large bias voltage “smooth”

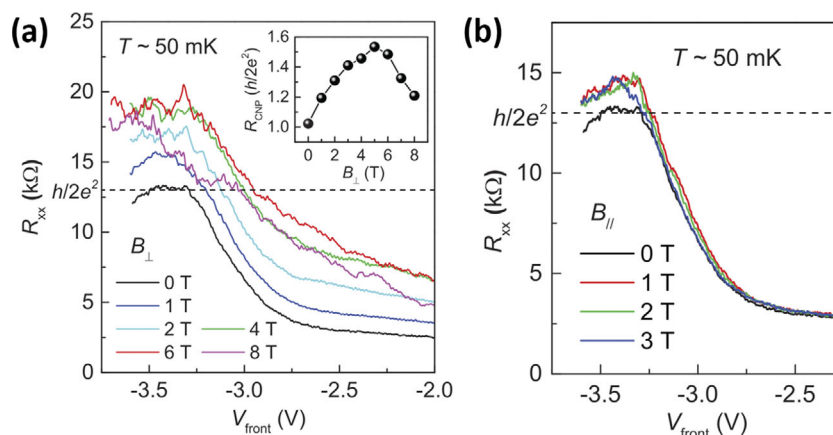


Figure 11. Resistance and its magnetic field response of strained InAs/GaSb quantum well in quantum spin Hall regime. Four-terminal resistance of strained-layer InAs/GaSb quantum well as a function of gate voltage under a) perpendicular and b) in-plane magnetic field in quantum spin Hall regime. The plateau resistances are close to $h/2e^2$ at zero field and increase when a magnetic field (< 5 T) is applied. At higher magnetic field, the plateau values decrease, which can be explained as a transition from helical edge states to chiral edge states. Inset: the resistance of charge neutral point as a function of perpendicular magnetic field. Reproduced with permission.^[55] Copyright 2017, APS.

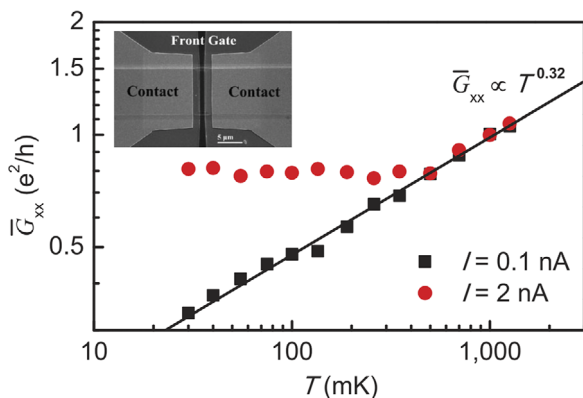


Figure 12. Luttinger liquid behavior in quantum spin Hall edge states. Temperature dependence of edge conductance in Si doped InAs/GaSb quantum well. The straight line indicates a power-law behavior $\bar{G}_{xx} \propto T^{0.32}$ for small excitation current, in contrast with helical edge conductance under large excitation current, which is temperature-independent under sufficient low temperature. This behavior can be explained as electron–electron interaction breaks the helical edge into segments. Reproduced with permission.^[63] Copyright 2015, APS.

the potential barriers that cut the edge state into segments and destroy the helical Luttinger liquid state.

By applying a vertical electric field, the quantum well can be tuned between conventional insulator and QSH insulator.^[49] The predicted “ON” and “OFF” of the QSH effect in InAs/GaSb quantum wells are demonstrated in refs. [64,65]. In these works, such transition is demonstrated by a large enhancement/depression of the resistance for samples in the hybridization gap. However, the predicted QSH resistance plateau is not observed in their works. Ref. [66] reports trivial edge channels in trivial regime of InAs/GaSb quantum wells, which may be confused with QSH edge states.

3. Quantum Spin Hall Effect in Layered Materials and Thin Films

The discovery of graphene^[5] opened the door of 2D materials research; and interestingly, the quest for QSH effect also started from graphene.^[19] Even though graphene in itself does not have the physical conditions necessary to support realistic QSH states, and even though semiconductor quantum well systems have taken the trophy of being the first experimentally realized QSH systems, the 2D materials and thin film material family is catching up fairly quickly. 2D QSH materials with strong experimental evidence includes monolayer WTe₂,^[59,67] Bismuthene,^[68] and Na₃Bi ultrathin film.^[69] There are also attractive theoretical proposals of QSH materials^[70–72] such as other monolayer transition metal dichalcogenides MX₂ (M = (W, Mo) and X = (Te, Se, S)),^[73] graphene heterostructures with strong spin–orbit coupling 2D materials,^[74] etc. Measurements at the step edges of bulk materials also provide evidence of the existence of edge conduction.^[75–77] This section mainly reviews experimental results of these materials.

3.1. Transition Metal Dichalcogenides

Monolayer transition metal dichalcogenides MX₂ (M = (W, Mo) and X = (Te, Se, S)) possess several atomic structures, such as 1T, 1T′, and 2H (or 1H for emphasizing the monolayer form),^[78–80] among which, the QSH effect was predicted in a number of monolayer 1T′-MX₂.^[73,81] Figure 13 shows the calculation results^[73] of 1T′-MX₂. The band structure near the Γ point shows the camelback shape, suggesting band inversion with an inverted gap 2δ . In 1T-MX₂, the conducting band consists of the *d*-orbitals of the transition metal atoms and the valence band consists of the *p*-orbitals of the chalcogen atoms. It is shown that in these materials, the 1T crystal structure is susceptible to a spontaneous lattice distortion in the *x* direction to form a period-doubling 2×1 distorted structure (called 1T′). Such distortion is found^[73] to cause the inversion of the *d*-orbitals and *p*-orbitals. Although the ground state of MX₂ is the 2H phase except for WTe₂, 1T′-MX₂ is metastable and there is an energy barrier between it and the 2H phase (see Figure 14a). Such energy barrier, together with the interaction between thin flake crystals and the substrate, could contribute to the fact that 1T′-MX₂ crystals can be directly synthesized;^[82–84] in addition, the conversion from the 2H phase to the 1T′ phase and its reverse process are both possible via similar physical treatment, such as thermal annealing and laser irradiation.^[85,86] Specifically, in ref. [82], it is reported that high-phase-purity 1T′-MoS₂ and MoSe₂ crystals can be synthesized and be exfoliated into 1T′ thin flakes. Then, these flakes can then be converted to the 2H phase by thermal annealing or by laser irradiation. In two other experiments, it is reported that 2H-MoTe₂^[85] and MoS₂^[86] can be converted to the 1T′ phase by laser irradiation. In ref. [85], 2H-MoTe₂ is mechanically exfoliated into multilayer flakes. Laser irradiation reduces the flake thickness and the phase transition between 2H and 1T′ phase occurs at the top layer of the irradiated area. The thinning down process continued until few-layer 1T′-MoTe₂ crystals remain on the substrate, which may be protected by heat dissipation to the substrate. Such 1T′-MoTe₂ is reported to be stable up to 300 °C. This technique is also performed on 2H-MoS₂ with similar results.^[86]

Monolayer 1T′-WTe₂ was initially calculated^[73] to be a semimetal, with a negative fundamental bulk gap evident in Figure 13c. This is less desirable since such band structure would mean that the helical edge states will be mixed with the conducting bulk states, and would be difficult to detect and to explore. The authors of ref. [73] proposed to open a positive gap by strain, which could be achieved by appropriate substrates or capping layers (see Figure 14b).^[73,87] Later on, a hybrid functional calculation is performed to show that, after consideration of many-body interactions and spin–orbit coupling, monolayer 1T′-WTe₂ actually has a large and positive band gap.^[88] Experimentally, after some early attempts^[88,89] on thin WTe₂ flakes, the insulating bulk and conducting edges are confirmed by angle-resolved photoemission (ARPES) study,^[67] scanning tunneling microscopy (STM)/scanning tunneling spectroscopy (STS) studies,^[67,90] SQUID current imaging study,^[91] and resistivity measurement.^[59,92]

As the most recent progress, clear quantized resistivity plateaus in monolayer 1T′-WTe₂ were reported in ref. [59]. Resistivity measurements were performed in a specially designed device geometry that overcome the electrical contact problem

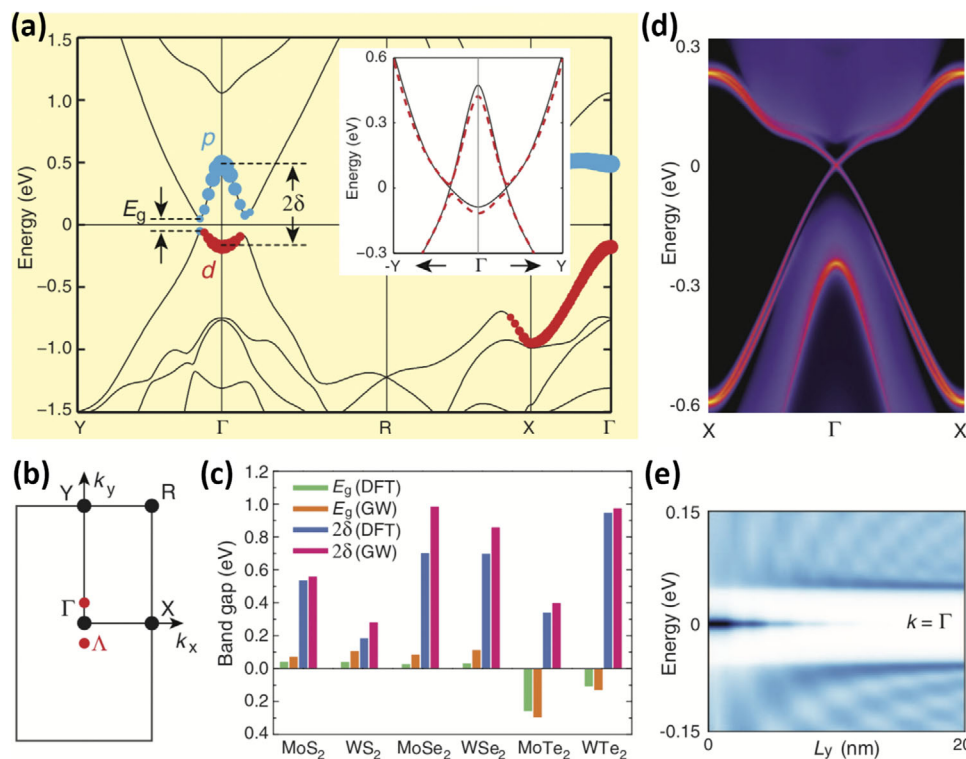


Figure 13. Calculated band structures of 1T' transition metal dichalcogenides. a) Band structure of 1T'-MoS₂. Inset: band structures with (dash) and without (solid) spin-orbit coupling. Near the Γ point, the valence band mainly consists of d-orbitals and the conduction band mainly consists of p-orbitals. b) Brillouin zone. The locations of the fundamental gap (E_g) are marked by red dots. c) Fundamental gap (E_g) and inverted gap (2δ) of all six 1T'-MX₂ (M = tungsten or molybdenum and X = tellurium, selenium, or sulfur). d) Edge density of states. e) Local density of states near at the Γ point as a function of distance away from the edge. Reproduced with permission.^[73] Copyright 2014, AAAS.

in the QSH regime using a combination of global top and local bottom gates, as shown in **Figure 15a**.^[59] The graphite top gate dopes a monolayer WTe₂ flake to the bulk-metallic state, ensuring ohmic contact whereas the local bottom gates tune part of the WTe₂ flake into the QSH regime. Such device structure

could effectively create a serial connection of one or a few high resistance sections in the QSH gapped regime with the majority of the sample in the low resistance (bulk-metallic) regime. As the defined QSH part is a short transport channel (≈ 100 nm), such design also ensures that the signal from a continuous edge

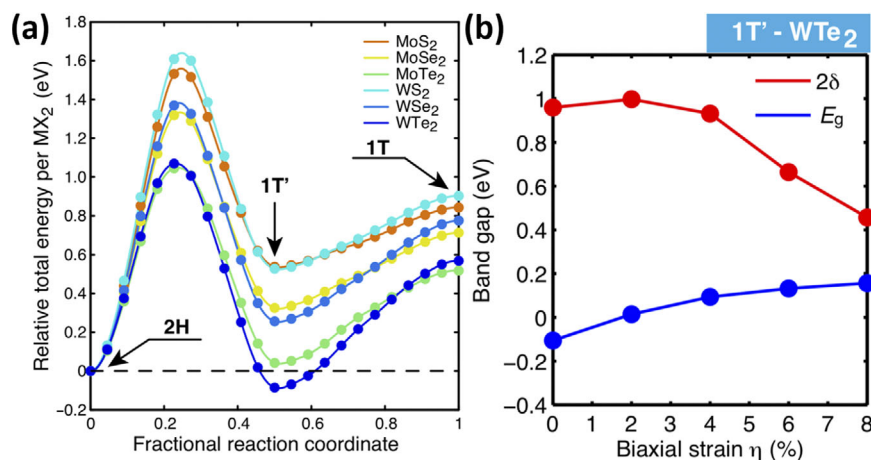


Figure 14. Structure stability and band gap tuning of monolayer transition metal dichalcogenides. a) Relative total energy per MX₂ as a function of fractional reaction coordinate. All MX₂ monolayers except WTe₂ are more stable in 2H structure. b) Effect of biaxial strain on fundamental gap (E_g) and inverted gap (2δ). Negative E_g indicates metal and positive E_g indicates insulator. Monolayer WTe₂ without strain is metal, which means the bulk remains conducting in quantum spin Hall regime. However, a small strain can open a gap in monolayer WTe₂, which can be realized by substrate. Reproduced with permission.^[73] Copyright 2014, AAAS.

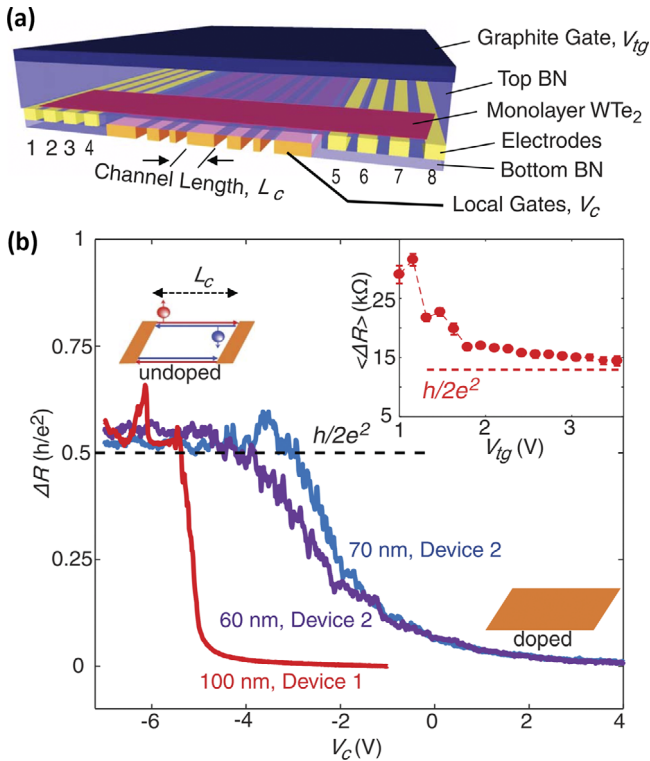


Figure 15. Resistance of monolayer $1T'$ - WTe_2 . a) Schematic of WTe_2 device structure. b) Offset resistance ($\Delta R = R(V_c) - R(V_c = -1 \text{ V})$) as a function of local gate voltage (V_c). The right two curves are offset by +3 V along the x axis. Resistance plateaus of $h/2e^2$ are clearly shown, indicating the channels doped by local gates are in quantum spin Hall states. Inset: the resistance plateau height as a function of top gate voltage (V_{tg}). For small V_{tg} , the carrier density in WTe_2 is low and the measured plateau resistance suffers from electrode contacts. Reproduced with permission.^[59] Copyright 2018, AAAS.

channel would be detected before the appearance of multiple segments in the helical edge states. Thus, when measuring resistivity of the $1T'$ - WTe_2 flake through the locally gated area, the resistivity changes from the highly doped limit to a quantized value $\Delta R = h/2e^2$ in the QSH regime (see Figure 15b). Using a series of local gates that define different QSH channel length, a length-dependent study of resistivity change ΔR rule out the possibility that trivial edge modes contributed to this quantized conductance value at a particular length (see Figure 15c). **Figure 16** plots the magnetic field dependence and temperature dependence of the QSH edge conductance.^[59] Suppression of channel's conductance was observed when applying a magnetic field. This suppression can be understood as the magnetic field opening a Zeeman gap at the Kramers degeneracy point of the QSH edge states.^[15] By performing temperature-dependence magnetoconductance measurement, a Zeeman-type gap opening is confirmed with an effective g -factor of ≈ 4.8 . This is the first report of Zeeman-type gap in the QSH regime. The $\Delta R = h/2e^2$ resistance plateau in WTe_2 survives up to 100 K, which is above liquid nitrogen temperature, makes the applications of the QSH effect more practical. This result is consistent with ARPES and STM measurements in which a large ($\approx 45 \text{ meV}$) bulk band gap was observed in monolayer WTe_2 .^[67,90]

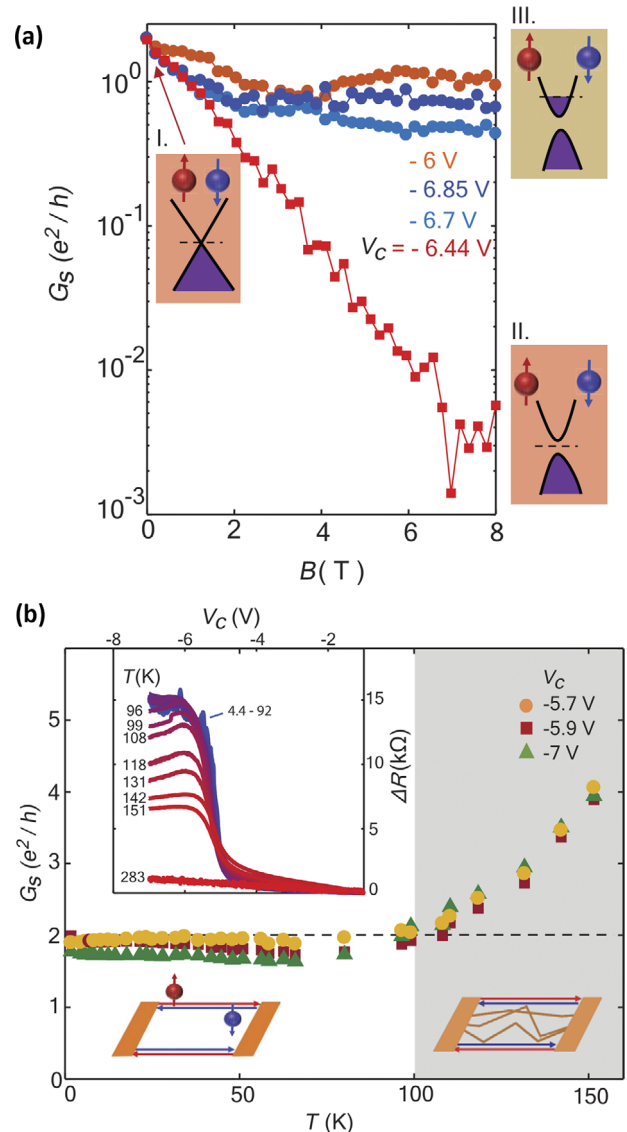


Figure 16. Magnetic field and temperature dependence of edge conductance in $1T'$ - WTe_2 . a) Edge conductance G_s as a function of magnetic field B at selected local gate voltages V_c . The nonsaturating behavior indicates the Fermi surface is in the Zeeman-like gap in quantum spin Hall edge states, as shown in insets I and II. b) Temperature dependence of the edge conductance at selected local gate voltages. The quantum spin Hall plateau survives up to 100 K. Inset: local gate dependence of offset resistance at various temperatures. The resistance plateau is roughly temperature-independent up to 92 K. Reproduced with permission.^[59] Copyright 2018, AAAS.

Besides the physical edges of MX_2 , the $1T'$ - $2H$ lateral interface can be regarded as the edge of $1T'$ - MX_2 , as the $2H$ phase is a semiconducting phase. Previously mentioned laser-induced phase patterning technique can create hetero-phase homojunctions between $2H$ and $1T'$ phase. Measurements on laser-patterned $1T'$ - MoS_2 show peak resistances near the helical edge transport value, where the edge is defined by the interface between $1T'$ and $2H$ phases.^[86] The existence of interface edge states is confirmed by STS spectra and the peak resistance

is temperature-independent below 25 K, which may point to the existence of QSH states. However, resistance plateaus are not reported, which may be due to sample's roughness caused by the laser irradiation process.

3.2. Other Materials

In addition to monolayer transition metal dichalcogenides MX_2 , layered transition metal pentatelluride ZrTe_5 and HfTe_5 have also been predicted as QSH insulators, with the added advantage of low interlayer binding energies which facilitates the exfoliation of the crystal down to the single layer.^[93] The predicted 0.1 eV QSH indirect band gap points to promising high-temperature applications of QSH states in these materials. Using STM/STS and ARPES measurements, edge states were observed at the surface step edges of bulk ZrTe_5 .^[75,77] Some efforts have been made on transport study of few-layer ZrTe_5 ;^[94,95] however, transport evidence of QSH effect in ZrTe_5 has not been reported.

Another direction in the search of QSH materials is to look for graphene like materials with strong spin-orbit coupling. Calculations show that the honeycomb-layer materials using Si, Ge, Sn have sufficiently large QSH gaps.^[96–99] However, these materials in freestanding form suffer from poor chemical stability. Practically, a supporting substrate is required. For example, silicene can be synthesized on Ag(111) surface.^[100] Unfortunately, a conducting substrate will short-circuit any edge states. Germanene and stanene can be synthesized on semiconducting materials, MoS_2 and Bi_2Te_3 , respectively.^[101,102] However, the synthesized samples are metallic, likely due to the strain from lattice constant mismatch between the substrates and the samples, thus the short-circuit problem remains. $\text{Bi}_{14}\text{Rh}_3\text{I}_9$ is proposed to be consisting of graphene-like QSH insulator layers sandwiched by trivial insulator spacers.^[103] Experimentally, a band gap has been observed by ARPES which was interpreted to be the QSH gap of the sample^[103] and edge conduction channels are observed by STS at the step edges of the bulk crystals of $\text{Bi}_{14}\text{Rh}_3\text{I}_9$.^[76]

Organic material is another class of predicted QSH materials, which has complex 2D lattice geometry. Generally, the building blocks are organometallic compounds which consist of C-metal and C–C bonds, such as $\text{Pb}(\text{C}_6\text{H}_5)_3$.^[104] In this particular compound, Pb atoms form a honeycomb lattice and benzene rings are inserted between adjacent Pb atoms with C-metal bonds. The QSH gap is calculated to be ≈ 8.6 meV. $\text{Ni}_3\text{C}_{12}\text{S}_{12}$ is a predicted organic QSH material in Kagome geometry, which has an SOC-induced gap ≈ 14 meV.^[105] The Kagome lattice of Cu-dicyanoanthracene is predicted to be an intrinsic QSH insulator.^[106] Here, intrinsic means that the Fermi surface is near the QSH gap and heavy doping is not required to obtain an insulating bulk. By replacing the metal atoms in organic QSH materials, the QSH gap can be tuned^[104–106] and quantum anomalous Hall effect may be induced.^[107] Synthesizing of such metal-organic materials have been reported^[108,109] but evidence of the existence of QSH states is yet to be obtained.

Freestanding bismuthene is a trivial insulator. However, according to calculation, when it is attached to proper substrates, such as Si(111) and SiC(0001), it could turn into a QSH insulator.^[110,111] The substrate converts the topological trivial bis-

muthene into a QSH insulator, which is called “substrate orbital filtering effect”. Such QSH edge states are examined in ref. [68]. ARPES measurement shows that the band gap in this system is ≈ 0.43 eV, while STS study confirms the existence of edge conducting channels. However, the topological character of the edge states is yet to be confirmed. Similar mechanism can be extended to other systems, such as trigonal Au on GaAs(111) surface, which is predicted to have a QSH gap of ≈ 73 meV.^[112]

Monolayer FeSe has been predicted to host helical edge states^[25,113] and the existence of edge conduction channels is experimentally identified by ARPES and STS measurements.^[25] In this system, TR symmetry is broken but the symmetry of combined TR and primitive-lattice-translation is preserved, which protects the edge states. This unconventional “QSH state” is called antiferromagnetic (AFM) QSH state. STS measurements show the existence of edge states along [100] and $[\bar{1}\bar{1}0]$ directions.^[25] Similar edge states are also reported in the domain boundaries of FeSe.^[114] Freestanding monolayer FeSe is predicted to be an intrinsic AFM QSH insulator, which means that the Fermi surface is in the SOC gap. Experimentally, the substrate $\text{SrTiO}_3(001)$ dopes the sample and the SOC gap lies under the Fermi surface.^[25] As $\text{FeSe}/\text{SrTiO}_3$ is reported to be a superconductor with high T_c ,^[115,116] it is possible to build a superconductor-AFM QSH insulator junction using one material. Furthermore, a quantum anomalous Hall (QAH) state is proposed to exist in monolayer FeSe under laser irradiation, which may provide opportunity in generating Majorana fermions in this material.^[117]

Apart from layered or 2D materials, several 3D materials were predicted to be QSH insulators at the ultrathin form, such as Bi ,^[118,119] transition metal oxide Na_2IrO_3 ,^[120] Si_2Te_2 ,^[121] as well as 3D topological Dirac semimetals Cd_3As_2 ^[122] and Na_3Bi .^[123] Recently, QSH effect was observed in mono- and bilayer films of Na_3Bi .^[69] Few-layer $\text{Na}_3\text{Bi}(001)$ was grown on Si(111) substrate, which has been demonstrated to have “ON” and “OFF” features by applying vertical electric field (see Section 2.2 for discussions on driving the transition between topologically nontrivial and topologically trivial states in QSH materials). **Figure 17b** plots the bandgap as a function of the electric field applied perpendicular to the Na_3Bi ultrathin film. The bandgap is extracted from the STS spectra and a critical electric field ≈ 1.1 V nm⁻¹ is shown above which the material will turn into a trivial insulator. The electric field is tuned by changing the distance between the STM tip and the Na_3Bi ultrathin film.^[69]

4. Creating Quantum Spin Hall States in Graphene

As mentioned in earlier sections, QSH effect is firstly predicted in graphene.^[19] Unfortunately, due to the weak spin orbit coupling, QSH effect in pristine graphene can only be observed at temperature $T \ll 0.01$ K according to the estimation in ref. [37]. Thus, the majority of effort in the field has been focused on other materials with stronger spin-orbit coupling^[39,59] or with peculiar band alignment configurations.^[40] Nonetheless, a substantial amount of attention in the field has remained focused on the study of graphene, which is not completely out of a sensation of reminiscence. Graphene still has an edge in the search for QSH candidate, because of its high crystal quality,^[124] high

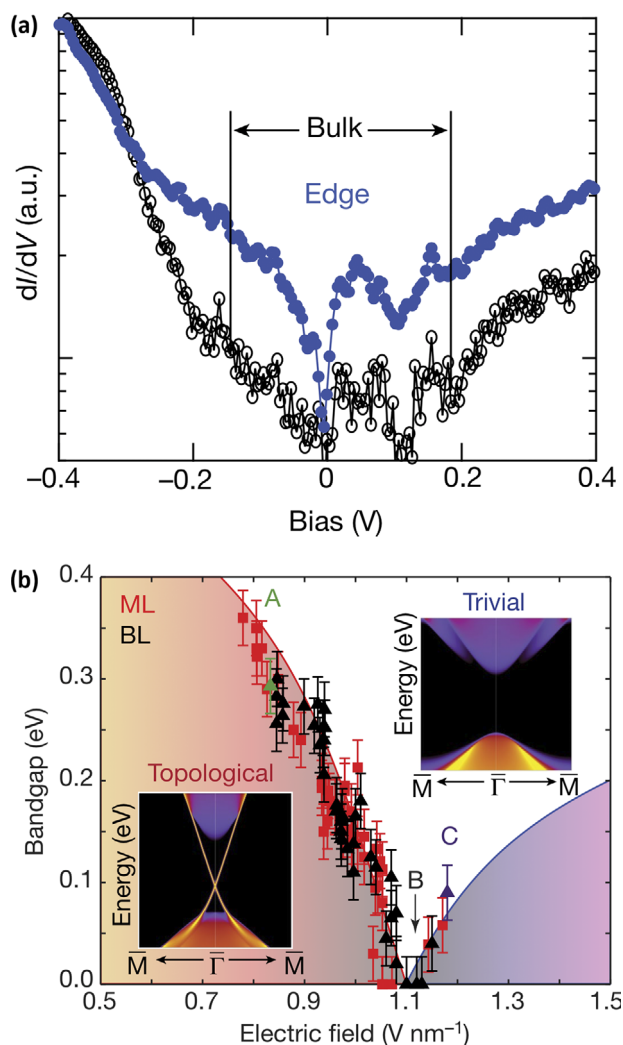


Figure 17. Bandgap in ultrathin Na₃Bi and edge state behavior under electric field. a) dI/dV spectra taken near the step edge of bilayer Na₃Bi to Si(111) substrate (blue) and in the bulk of bilayer Na₃Bi (black). The spectrum at edge is quite different from that at bulk, indicating existence of edge states. b) Bandgap extracted from dI/dV spectra as a function of electric field. Squares and triangles represent monolayer and bilayer bandgap, respectively. The electric field is controlled by tip-sample separation, as there is a difference in work function between the tip and the sample. The electric field close the quantum spin Hall bandgap and re-open it as a trivial insulator. Reproduced with permission.^[69] Copyright 2018, Springer Nature.

electron/hole mobility,^[125] chemical stability, high sensitivity to interfacial tuning,^[126] and an easy device fabrication process. This section reviews works on realizing helical edge states in graphene.

4.1. Adatoms and Decoration

Some adatoms on graphene can be regarded as spin-orbit coupling or spin-orbit scattering sources.^[127,128] This can be understood by considering the process that an electron in graphene tunnels into an adatom, then returns to the graphene. If the tun-

neling process is spin-dependent, it can locally enhance spin-orbit coupling. Spin-orbit coupling in graphene includes intrinsic coupling which induces QSH effect and Rashba coupling which prevents QSH effect.^[19] In order to increase QSH temperature in graphene, the adatoms should mainly induce intrinsic (Kane–Mele type) spin-orbit coupling.^[129] Theory predicted indium and thallium adatoms could stabilize a robust QSH state in graphene with only a few percent of coverage.^[130,131] Osmium, iridium adatoms and tellurium edge decoration-induced QSH effects are also predicted.^[132,133] Transport studies of graphene with indium adatoms^[134,135] and iridium adatoms^[136] were performed; however, no evidence of QSH effect was reported, possibly due to the clustering of adatoms^[137,138] or surface contaminations. Indeed, the adatom decoration process is realized by setting up an evaporation source inside a conventional cryostat,^[134,135] during which the surface conditions of the graphene sample are less controlled. Recently, a study on Bi₂Te₃ decorated graphene reports resistivity peak values qualitatively agree with helical edge transport result.^[139] The authors attribute this behavior to spin-orbit coupling induced by Bi₂Te₃.^[140] QSH effect is also predicted in graphene interacting with single crystal WS₂ or WSe₂.^[74] Experimentally, such heterostructures show promising features with a substantial enhancement in the spin-orbit coupling strength in graphene.^[141–145]

4.2. Construct Helical Edge States by Landau Levels

The QH effect in graphene occurs up to room temperature for its large Landau level (LL) gaps.^[146] Unlike the QSH effect, the edge states of QH effect propagate in one direction with their spin states degenerated. Under a strong magnetic field, the edge states will split into spin-up and spin-down states due to the Zeeman effect. If an edge contains two edge states with different spin and different propagating directions, it behaves like edge states in the QSH effect and is protected by CT invariance (C represents charge conjugation operation and T stands for the TR operation).^[147] The only difference is that such modes are not supported by the spin-orbit coupling but by the strong magnetic field. In QH effect, the propagating direction is determined by the types of charge carriers under the same static magnetic field. In other words, helical edge states can be built by superimposing an electron LL and a hole LL with different spin polarizations. This can be realized in charge neutral graphene in a strong magnetic field. LL at zero energy in graphene has fourfold degeneracy^[148] due to the spin and valley degrees of freedom. This LL is half-filled for charge-neutral graphene. In strong magnetic field, the zeroth LL splits due to the Zeeman effect and it is expected to cause helical edge states at charge neutrality.

However, graphene at charge neutrality shows insulating behavior under a perpendicular magnetic field. This arises due to an unexpected spin polarization which is called “quantum Hall ferromagnetism.”^[148] Since an in-plane magnetic field generates Zeeman splitting without breaking other symmetry, a tilted magnetic field is proposed to realize helical edge states in graphene. The perpendicular magnetic field should be small compared to the parallel magnetic field so that the Zeeman splitting is dominant compared with the symmetry breaking gap; on the other hand, the perpendicular magnetic field should be large enough

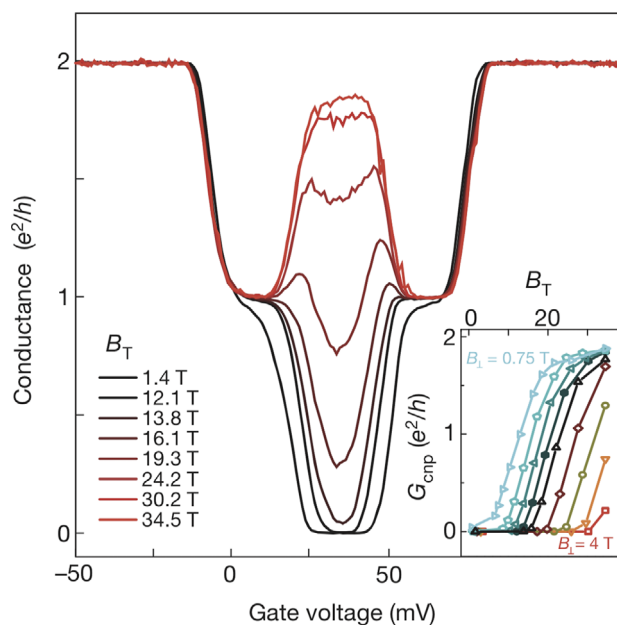


Figure 18. Conductance of $\nu = 0$ state in graphene with an in-plane magnetic field. Conductance at perpendicular magnetic field $B_{\perp} = 1.4$ T as a function of gate voltage at different total magnetic fields B_T . The $\nu = 0$ state is insulating at low in-plane magnetic field and gradually becomes conducting as the in-plane magnetic field increases. The conductance saturating at $G \approx 1.8e^2/h$ at high magnetic field, which is close to helical edge conductance $2e^2/h$. Inset: charge neutral point conductance as a function of B_T at selected B_{\perp} (0.75, 1.0, 1.4, 1.6, 2.0, 2.5, 3.0, 4.0 T). A saturating behavior is shown. Reproduced with permission.^[24] Copyright 2014, Nature Publishing Group.

so that the QH states are well defined. Though TR symmetry is broken by magnetic field in this system, the helical edge states are protected by U(1) symmetry of electron spin rotations.^[24]

Ref. [24] reports an increasing conductance at the charge-neutral point of single layer graphene in the QH regime with increasing in-plane magnetic field (see **Figure 18**). The conductance stops increasing at $G = 1.8e^2/h$ for the largest magnetic field they applied. Simultaneous capacitance measurement implies that the bulk is insulating while the measured conductance is nonzero. The authors concluded that such conductance is the evidence of the existence of helical edge states.

Along the direction discussed in the first paragraph of Section 4.2, one can also try to construct helical edge states using twisted bilayer graphene. The twisted stacking decreases the interlayer coupling, so that the edge states could be independent in each layer. By applying perpendicular magnetic field and gating one layer into the $n = 1$ QH plateau and the other into the $n = -1$ QH plateau, a pair of helical edge states can be constructed. Transport data^[149] of such system is shown in **Figure 19**. The backscattering between the two QH edge states is suppressed, supported by the high conductance plateau at the $(+1/-1)$ states. In contrast, the conductance at the $(+2/-2)$ states is much lower. One advantage in this system is that the helical edge states can be constructed by fractional QH edge states, which may pave the way toward fractional QSH effect.

As can be seen from the above discussions, the methods to construct QSH-like states under high magnetic field and high-

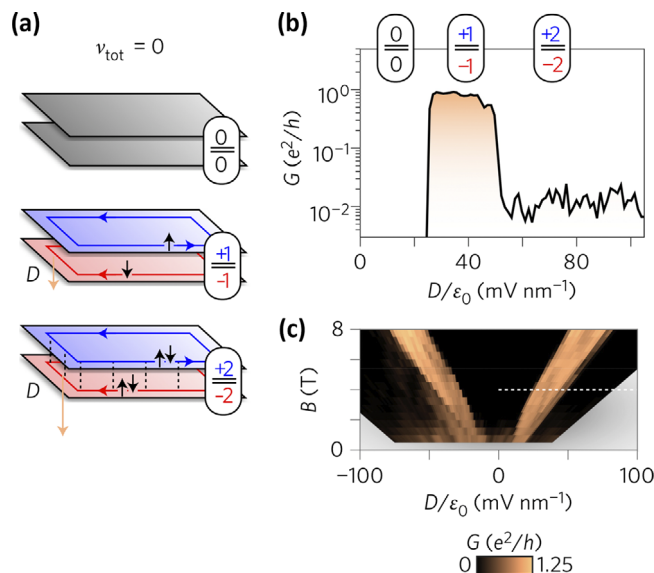


Figure 19. Conductance in graphene electron-hole quantum Hall bilayers. a) Schematic of edge states in graphene electron-hole bilayers. The bilayer is twisted to reduce interlayer coupling. Both layers are in quantum Hall states and charge neutral ($\nu_{\text{bottom}} = -\nu_{\text{top}}$ and $\nu_{\text{tot}} = \nu_{\text{bottom}} + \nu_{\text{top}} = 0$). Such state is labeled as $(\nu_{\text{top}}, \nu_{\text{bottom}})$. The $(+1, -1)$ state can be regarded as helical edge state. b) Two-terminal conductance for $\nu_{\text{tot}} = 0$ as a function of displacement field at $B = 4$ T. The $(+1, -1)$ state is conductive while the $(+2, -2)$ state is insulating, indicating the backscattering in this state is suppressed. c) Two-probe conductance in magnetic field-displacement field plane. Dash line indicates $\nu_{\text{tot}} = 0$ and contact resistances are subtracted. Reproduced with permission.^[149] Copyright 2017, Springer Nature.

mobility graphene heterostructures, represented a powerful technique in controlling electronic system, and can form a basis for mixing QSH effect with other mesoscopic concepts such as exciton condensation.^[150–153]

5. Conclusion

In summary, this article aims to provide an up-to-date review on the exciting development of the quantum spin Hall effect with an emphasis in the material aspects. A clear trend in the field is that substantial progress has been made with the synergetic efforts from both the theoretical community and the experimental community. Newer, better materials drive the development in this scientific area. In the future, it is expected that more QSH materials will be discovered, and the temperature in which QSH effect works will get higher. If everything progresses smoothly, the construction of Majorana Fermions and topological quantum computation using QSH-based heterostructures seems to be within reach in the near future.

Acknowledgements

This project has been supported by the National Basic Research Program of China (973 Grant Nos. 2018YFA0305604), the National Natural Science Foundation of China (NSFC Grant Nos. 11774010). C.C. and

J.-H.C. discussed the layout and content of the manuscript and wrote the manuscript together.

Conflict of Interest

The authors declare no conflict of interest.

Keywords

2D electron systems, helical edge states, low-dimensional systems, quantum spin Hall states, topological insulators

Received: March 25, 2019

Revised: May 31, 2019

Published online: July 11, 2019

-
- [1] K. Vonklitzing, G. Dorda, M. Pepper, *Phys. Rev. Lett.* **1980**, 45, 494.
- [2] H. L. Störmer, R. Dingle, A. C. Gossard, W. Wiegmann, M. D. Sturge, *Solid State Commun.* **1979**, 29, 705.
- [3] A. Ohtomo, H. Y. Hwang, *Nature* **2004**, 427, 423.
- [4] A. Tsukazaki, A. Ohtomo, T. Kita, Y. Ohno, H. Ohno, M. Kawasaki, *Science* **2007**, 315, 1388.
- [5] K. S. Novoselov, A. K. Geim, S. V. Morozov, D. Jiang, Y. Zhang, S. V. Dubonos, I. V. Grigorieva, A. A. Firsov, *Science* **2004**, 306, 666.
- [6] L. K. Li, Y. J. Yu, G. J. Ye, Q. Q. Ge, X. D. Ou, H. Wu, D. L. Feng, X. H. Chen, Y. B. Zhang, *Nat. Nanotechnol.* **2014**, 9, 372.
- [7] D. A. Bandurin, A. V. Tyurnina, G. L. Yu, A. Mishchenko, V. Zolyomi, S. V. Morozov, R. K. Kumar, R. V. Gorbachev, Z. R. Kudrynskiy, S. Pezzini, Z. D. Kovalyuk, U. Zeitler, K. S. Novoselov, A. Patane, L. Eaves, I. V. Grigorieva, V. I. Fal'ko, A. K. Geim, Y. Cao, *Nat. Nanotechnol.* **2017**, 12, 223.
- [8] B. Radisavljevic, A. Radenovic, J. Brivio, V. Giacometti, A. Kis, *Nat. Nanotechnol.* **2011**, 6, 147.
- [9] S. G. Xu, J. Y. Shen, G. Long, Z. F. Wu, Z. Q. Bao, C. C. Liu, X. Xiao, T. Y. Han, J. X. Z. Lin, Y. Y. Wu, H. H. Lu, J. Q. Hou, L. H. An, Y. W. Wang, Y. Cai, K. M. Ho, Y. H. He, R. Lortz, F. Zhang, N. Wang, *Phys. Rev. Lett.* **2017**, 118, 067702.
- [10] C. Zhang, Y. Zhang, X. Yuan, S. H. Lu, J. L. Zhang, A. Narayan, Y. E. Liu, H. Q. Zhang, Z. L. Ni, R. Liu, E. S. Choi, A. Suslov, S. Sanvito, L. Pi, H. Z. Lu, A. C. Potter, F. X. Xiu, *Nature* **2019**, 565, 331.
- [11] F. Tang, Y. Ren, P. Wang, R. Zhong, J. Schneeloch, S. A. Yang, K. Yang, P. A. Lee, G. Gu, Z. Qiao, L. Zhang, *arXiv:1807.02678v2*, **2018**.
- [12] J. Yin, S. Slizovskiy, Y. Cao, S. Hu, Y. Yang, I. Lobanova, B. A. Piot, S.-K. Son, S. Ozdemir, T. Taniguchi, K. Watanabe, K. S. Novoselov, F. Guinea, A. K. Geim, V. Fal'ko, A. Mishchenko, *Nat. Phys.* **2019**, 15, 437.
- [13] X.-L. Qi, S.-C. Zhang, *Phys. Today* **2010**, 63, 33.
- [14] J. Maciejko, T. L. Hughes, S. C. Zhang, *Annu. Rev. Condens. Matter Phys.* **2011**, 2, 31.
- [15] M. König, H. Buhmann, L. W. Molenkamp, T. Hughes, C.-X. Liu, X.-L. Qi, S.-C. Zhang, *J. Phys. Soc. Jpn.* **2008**, 77, 031007.
- [16] M. Z. Hasan, C. L. Kane, *Rev. Mod. Phys.* **2010**, 82, 3045.
- [17] X. L. Qi, S. C. Zhang, *Rev. Mod. Phys.* **2011**, 83, 1057.
- [18] C. L. Kane, E. J. Mele, *Phys. Rev. Lett.* **2005**, 95, 146802.
- [19] C. L. Kane, E. J. Mele, *Phys. Rev. Lett.* **2005**, 95, 226801.
- [20] B. A. Bernevig, S. C. Zhang, *Phys. Rev. Lett.* **2006**, 96, 106802.
- [21] B. A. Bernevig, T. L. Hughes, S. C. Zhang, *Science* **2006**, 314, 1757.
- [22] L. Sheng, D. N. Sheng, C. S. Ting, F. D. M. Haldane, *Phys. Rev. Lett.* **2005**, 95, 136602.
- [23] D. N. Sheng, Z. Y. Weng, L. Sheng, F. D. M. Haldane, *Phys. Rev. Lett.* **2006**, 97, 036808.
- [24] A. F. Young, J. D. Sanchez-Yamagishi, B. Hunt, S. H. Choi, K. Watanabe, T. Taniguchi, R. C. Ashoori, P. Jarillo-Herrero, *Nature* **2014**, 505, 528.
- [25] Z. F. Wang, H. M. Zhang, D. F. Liu, C. Liu, C. J. Tang, C. L. Song, Y. Zhong, J. P. Peng, F. S. Li, C. N. Nie, L. L. Wang, X. J. Zhou, X. C. Ma, Q. K. Xue, F. Liu, *Nat. Mater.* **2016**, 15, 968.
- [26] S. M. Albrecht, A. P. Higginbotham, M. Madsen, F. Kuemmeth, T. S. Jespersen, J. Nygard, P. Krogstrup, C. M. Marcus, *Nature* **2016**, 531, 206.
- [27] L. Fu, C. L. Kane, *Phys. Rev. B* **2007**, 76, 045302.
- [28] D. Hsieh, D. Qian, L. Wray, Y. Xia, Y. S. Hor, R. J. Cava, M. Z. Hasan, *Nature* **2008**, 452, 970.
- [29] H. A. Kramers, *Proc. Amsterdam Acad.* **1930**, 33, 959.
- [30] C. Nayak, S. H. Simon, A. Stern, M. Freedman, S. Das Sarma, *Rev. Mod. Phys.* **2008**, 80, 1083.
- [31] L. Fu, C. L. Kane, *Phys. Rev. B* **2009**, 79, 161408.
- [32] J. Nilsson, A. R. Akhmerov, C. W. J. Beenakker, *Phys. Rev. Lett.* **2008**, 101, 120403.
- [33] X. L. Qi, T. L. Hughes, S. C. Zhang, *Nat. Phys.* **2008**, 4, 273.
- [34] M. Cheng, *Phys. Rev. B* **2012**, 86, 195126.
- [35] N. H. Lindner, E. Berg, G. Refael, A. Stern, *Phys. Rev. X* **2012**, 2, 041002.
- [36] D. J. Clarke, J. Alicea, K. Shtengel, *Nat. Commun.* **2013**, 4, 1348.
- [37] H. Min, J. E. Hill, N. A. Sinitsyn, B. R. Sahu, L. Kleinman, A. H. MacDonald, *Phys. Rev. B* **2006**, 74, 165310.
- [38] Y. Yao, F. Ye, X.-L. Qi, S.-C. Zhang, Z. Fang, *Phys. Rev. B* **2007**, 75, 041401.
- [39] M. König, S. Wiedmann, C. Brune, A. Roth, H. Buhmann, L. W. Molenkamp, X. L. Qi, S. C. Zhang, *Science* **2007**, 318, 766.
- [40] L. J. Du, I. Knez, G. Sullivan, R. R. Du, *Phys. Rev. Lett.* **2015**, 114, 096802.
- [41] H. J. Zhang, C. X. Liu, X. L. Qi, X. Dai, Z. Fang, S. C. Zhang, *Nat. Phys.* **2009**, 5, 438.
- [42] A. Roth, C. Brune, H. Buhmann, L. W. Molenkamp, J. Maciejko, X. L. Qi, S. C. Zhang, *Science* **2009**, 325, 294.
- [43] S. Hart, H. Ren, T. Wagner, P. Leubner, M. Mühlbauer, C. Brune, H. Buhmann, L. Molenkamp, A. Yacoby, *Nat. Phys.* **2014**, 10, 638.
- [44] K. C. Nowack, E. M. Spanton, M. Baenninger, M. König, J. R. Kirtley, B. Kalisky, C. Ames, P. Leubner, C. Brune, H. Buhmann, L. W. Molenkamp, D. Goldhaber-Gordon, K. A. Moler, *Nat. Mater.* **2013**, 12, 787.
- [45] B. Buttner, C. X. Liu, G. Tkachov, E. G. Novik, C. Brune, H. Buhmann, E. M. Hankiewicz, P. Recher, B. Trauzettel, S. C. Zhang, L. W. Molenkamp, *Nat. Phys.* **2011**, 7, 418.
- [46] M. Zholudev, F. Tepe, M. Orlita, C. Consejo, J. Torres, N. Dyakonova, M. Czapkiewicz, J. Wrobel, G. Grabecki, N. Mikhailov, S. Dvoretiskii, A. Ikonnikov, K. Spirin, V. Aleshkin, V. Gavrilenko, W. Knap, *Phys. Rev. B* **2012**, 86, 205420.
- [47] M. Buttiker, *Phys. Rev. Lett.* **1986**, 57, 1761.
- [48] B. Zhou, H. Z. Lu, R. L. Chu, S. Q. Shen, Q. Niu, *Phys. Rev. Lett.* **2008**, 101, 246807.
- [49] C. X. Liu, T. L. Hughes, X. L. Qi, K. Wang, S. C. Zhang, *Phys. Rev. Lett.* **2008**, 100, 236601.
- [50] I. Knez, R. R. Du, G. Sullivan, *Phys. Rev. B* **2010**, 81, 201301.
- [51] I. Knez, R. R. Du, G. Sullivan, *Phys. Rev. Lett.* **2011**, 107, 136603.
- [52] I. Knez, R. R. Du, G. Sullivan, *Phys. Rev. Lett.* **2012**, 109, 186603.
- [53] K. Suzuki, Y. Harada, K. Onomitsu, K. Muraki, *Phys. Rev. B* **2013**, 87, 235311.
- [54] S. Mueller, A. N. Pal, M. Karalic, T. Tschirky, C. Charpentier, W. Wegscheider, K. Ensslin, T. Ihn, *Phys. Rev. B* **2015**, 92, 081303.
- [55] L. J. Du, T. X. Li, W. K. Lou, X. J. Wu, X. X. Liu, Z. D. Han, C. Zhang, G. Sullivan, A. Ikhlassi, K. Chang, R. R. Du, *Phys. Rev. Lett.* **2017**, 119, 056803.
- [56] F. Couedo, H. Irie, K. Suzuki, K. Onomitsu, K. Muraki, *Phys. Rev. B* **2016**, 94, 035301.

- [57] E. M. Spanton, K. C. Nowack, L. J. Du, G. Sullivan, R. R. Du, K. A. Moler, *Phys. Rev. Lett.* **2014**, *113*, 026804.
- [58] C. Charpentier, S. Falt, C. Reichl, F. Nichele, A. N. Pal, P. Pietsch, T. Ihn, K. Ensslin, W. Wegscheider, *Appl. Phys. Lett.* **2013**, *103*, 112102.
- [59] S. Wu, V. Fatemi, Q. D. Gibson, K. Watanabe, T. Taniguchi, R. J. Cava, P. Jarillo-Herrero, *Science* **2018**, *359*, 76.
- [60] C. J. Wu, B. A. Bernevig, S. C. Zhang, *Phys. Rev. Lett.* **2006**, *96*, 106401.
- [61] C. K. Xu, J. E. Moore, *Phys. Rev. B* **2006**, *73*, 045322.
- [62] J. Maciejko, C. X. Liu, Y. Oreg, X. L. Qi, C. J. Wu, S. C. Zhang, *Phys. Rev. Lett.* **2009**, *102*, 256803.
- [63] T. X. Li, P. J. Wang, H. L. Fu, L. J. Du, K. A. Schreiber, X. Y. Mu, X. X. Liu, G. Sullivan, G. A. Csathy, X. Lin, R. R. Du, *Phys. Rev. Lett.* **2015**, *115*, 136804.
- [64] F. M. Qu, A. J. A. Beukman, S. Nadj-Perge, M. Wimmer, B. M. Nguyen, W. Yi, J. Thorp, M. Sokolich, A. A. Kiselev, M. J. Manfra, C. M. Marcus, L. P. Kouwenhoven, *Phys. Rev. Lett.* **2015**, *115*, 036803.
- [65] K. Suzuki, Y. Harada, K. Onomitsu, K. Muraki, *Phys. Rev. B* **2015**, *91*, 245309.
- [66] F. Nichele, H. J. Suominen, M. Kjaergaard, C. M. Marcus, E. Sajadi, J. A. Folk, F. M. Qu, A. J. A. Beukman, F. K. de Vries, J. van Veen, S. Nadj-Perge, L. P. Kouwenhoven, B. M. Nguyen, A. A. Kiselev, W. Yi, M. Sokolich, M. J. Manfra, E. M. Spanton, K. A. Moler, *New J. Phys.* **2016**, *18*, 083005.
- [67] S. J. Tang, C. F. Zhang, D. Wong, Z. Pedramrazi, H. Z. Tsai, C. J. Jia, B. Moritz, M. Claassen, H. Ryu, S. Kahn, J. Jiang, H. Yan, M. Hashimoto, D. H. Lu, R. G. Moore, C. C. Hwang, C. Hwang, Z. Hussain, Y. L. Chen, M. M. Ugeda, Z. Liu, X. M. Xie, T. P. Devereaux, M. F. Crommie, S. K. Mo, Z. X. Shen, *Nat. Phys.* **2017**, *13*, 683.
- [68] F. Reis, G. Li, L. Dudy, M. Bauerfeind, S. Glass, W. Hanke, R. Thomale, J. Schafer, R. Claessen, *Science* **2017**, *357*, 287.
- [69] J. L. Collins, A. Tadich, W. Wu, L. C. Gomes, J. N. B. Rodrigues, C. Liu, J. Hellerstedt, H. Ryu, S. Tang, S.-K. Mo, S. Adam, S. A. Yang, M. S. Fuhrer, M. T. Edmonds, *Nature* **2018**, *564*, 390.
- [70] Y. F. Ren, Z. H. Qiao, Q. Niu, *Rep. Prog. Phys.* **2016**, *79*, 066501.
- [71] Z. F. Wang, K. H. Jin, F. Liu, *Wires Comput. Mol. Sci.* **2017**, *7*, e1304.
- [72] L. Z. Kou, Y. D. Ma, Z. Q. Sun, T. Heine, C. F. Chen, *J. Phys. Chem. Lett.* **2017**, *8*, 1905.
- [73] X. F. Qian, J. W. Liu, L. Fu, J. Li, *Science* **2014**, *346*, 1344.
- [74] T. P. Kaloni, L. Kou, T. Frauenheim, U. Schwingenschlogl, *Appl. Phys. Lett.* **2014**, *105*, 233112.
- [75] X. B. Li, W. K. Huang, Y. Y. Lv, K. W. Zhang, C. L. Yang, B. B. Zhang, Y. B. Chen, S. H. Yao, J. Zhou, M. H. Lu, L. Sheng, S. C. Li, J. F. Jia, Q. K. Xue, Y. F. Chen, D. Y. Xing, *Phys. Rev. Lett.* **2016**, *116*, 176803.
- [76] C. Pauly, B. Rasche, K. Koepf, M. Liebmann, M. Pratzner, M. Richter, J. Kellner, M. Eschbach, B. Kaufmann, L. Plucinski, C. M. Schneider, M. Ruck, J. van den Brink, M. Morgenstern, *Nat. Phys.* **2015**, *11*, 338.
- [77] R. Wu, J. Z. Ma, S. M. Nie, L. X. Zhao, X. Huang, J. X. Yin, B. B. Fu, P. Richard, G. F. Chen, Z. Fang, X. Dai, H. M. Weng, T. Qian, H. Ding, S. H. Pan, *Phys. Rev. X* **2016**, *6*, 021017.
- [78] J. Heising, M. G. Kanatzidis, *J. Am. Chem. Soc.* **1999**, *121*, 638.
- [79] G. Eda, T. Fujita, H. Yamaguchi, D. Voiry, M. W. Chen, M. Chhowalla, *ACS Nano* **2012**, *6*, 7311.
- [80] Y. Wang, J. Xiao, H. Y. Zhu, Y. Li, Y. Alsaied, K. Y. Fong, Y. Zhou, S. Q. Wang, W. Shi, Y. Wang, A. Zettl, E. J. Reed, X. Zhang, *Nature* **2017**, *550*, 487.
- [81] Y. D. Ma, L. Z. Kou, X. Li, Y. Dai, S. C. Smith, T. Heine, *Phys. Rev. B* **2015**, *92*, 085427.
- [82] Y. Yu, G.-H. Nam, Q. He, X.-J. Wu, K. Zhang, Z. Yang, J. Chen, Q. Ma, M. Zhao, Z. Liu, F.-R. Ran, X. Wang, H. Li, X. Huang, B. Li, Q. Xiong, Q. Zhang, Z. Liu, L. Gu, Y. Du, W. Huang, H. Zhang, *Nat. Chem.* **2018**, *10*, 638.
- [83] C. H. Naylor, W. M. Parkin, J. L. Ping, Z. L. Gao, Y. R. Zhou, Y. Kim, F. Streller, R. W. Carpick, A. M. Rappe, M. Drndic, J. M. Kikkawa, A. T. C. Johnson, *Nano Lett.* **2016**, *16*, 4297.
- [84] K. Deng, G. L. Wan, P. Deng, K. N. Zhang, S. J. Ding, E. Y. Wang, M. Z. Yan, H. Q. Huang, H. Y. Zhang, Z. L. Xu, J. Denlinger, A. Fedorov, H. T. Yang, W. H. Duan, H. Yao, Y. Wu, S. S. Fan, H. J. Zhang, X. Chen, S. Y. Zhou, *Nat. Phys.* **2016**, *12*, 1105.
- [85] S. Cho, S. Kim, J. H. Kim, J. Zhao, J. Seok, D. H. Keum, J. Baik, D. H. Choe, K. J. Chang, K. Suenaga, S. W. Kim, Y. H. Lee, H. Yang, *Science* **2015**, *349*, 625.
- [86] A. K. H. Mine, T. Nakamura, T. Inoue, S. Pakdel, E. Z. Marin, D. Mariani, E. Gonzalez-Marín, S. Maruyama, S. Katsumoto, A. Fortunelli, J. J. Palacios, J. Haruyama, *arXiv:1807.04914v2*, **2018**.
- [87] M. A. Cazalilla, H. Ochoa, F. Guinea, *Phys. Rev. Lett.* **2014**, *113*, 077201.
- [88] F. P. Zheng, C. Y. Cai, S. F. Ge, X. F. Zhang, X. Liu, H. Lu, Y. D. Zhang, J. Qiu, T. Taniguchi, K. Watanabe, S. Jia, J. S. Qi, J. H. Chen, D. Sun, J. Feng, *Adv. Mater.* **2016**, *28*, 4845.
- [89] J. Lee, F. Ye, Z. H. Wang, R. Yang, J. Hu, Z. Q. Mao, J. Wei, P. X. L. Feng, *Nanoscale* **2016**, *8*, 7854.
- [90] Z. Y. Jia, Y. H. Song, X. B. Li, K. J. Ran, P. C. Lu, H. J. Zheng, X. Y. Zhu, Z. Q. Shi, J. Sun, J. S. Wen, D. Y. Xing, S. C. Li, *Phys. Rev. B* **2017**, *96*, 041108.
- [91] Y. Shi, J. Kahn, B. Niu, Z. Fei, B. Sun, X. Cai, B. A. Francisco, D. Wu, Z.-X. Shen, X. Xu, D. H. Cobden, Y.-T. Cui, *Sci. Adv.* **2019**, *5*, eaat8799.
- [92] Z. Fei, T. Palomaki, S. Wu, W. Zhao, X. Cai, B. Sun, P. Nguyen, J. Finney, X. Xu, D. H. Cobden, *Nat. Phys.* **2017**, *13*, 677.
- [93] H. M. Weng, X. Dai, Z. Fang, *Phys. Rev. X* **2014**, *4*, 011002.
- [94] G. Qiu, Y. C. Du, A. Charnas, H. Zhou, S. Y. Jin, Z. Luo, D. Y. Zemlyanov, X. F. Xu, G. J. Cheng, P. D. D. Ye, *Nano Lett.* **2016**, *16*, 7364.
- [95] J. J. Niu, J. Y. Wang, Z. J. He, C. L. Zhang, X. Q. Li, T. C. Cai, X. M. Ma, S. Jia, D. P. Yu, X. S. Wu, *Phys. Rev. B* **2017**, *95*, 035420.
- [96] C. C. Liu, W. X. Feng, Y. G. Yao, *Phys. Rev. Lett.* **2011**, *107*, 076802.
- [97] Y. Xu, B. H. Yan, H. J. Zhang, J. Wang, G. Xu, P. Z. Tang, W. H. Duan, S. C. Zhang, *Phys. Rev. Lett.* **2013**, *111*, 136804.
- [98] C. C. Liu, H. Jiang, Y. G. Yao, *Phys. Rev. B* **2011**, *84*, 195430.
- [99] Y. P. Wang, W. X. Ji, C. W. Zhang, P. Li, F. Li, P. J. Wang, S. S. Li, S. S. Yan, *Appl. Phys. Lett.* **2016**, *108*, 073104.
- [100] P. Vogt, P. De Padova, C. Quaresima, J. Avila, E. Frantzeskakis, M. C. Asensio, A. Resta, B. Ealet, G. Le Lay, *Phys. Rev. Lett.* **2012**, *108*, 155501.
- [101] L. Zhang, P. Bampoulis, A. N. Rudenko, Q. Yao, A. van Houselt, B. Poelsema, M. I. Katsnelson, H. J. W. Zandvliet, *Phys. Rev. Lett.* **2016**, *116*, 256804.
- [102] F.-F. Zhu, W.-J. Chen, Y. Xu, C.-L. Gao, D.-D. Guan, C.-H. Liu, D. Qian, S.-C. Zhang, J.-F. Jia, *Nat. Mater.* **2015**, *14*, 1020.
- [103] B. Rasche, A. Isaeva, M. Ruck, S. Borisenko, V. Zabolotnyy, B. Buchner, K. Koepf, C. Ortix, M. Richter, J. van den Brink, *Nat. Mater.* **2013**, *12*, 422.
- [104] Z. F. Wang, Z. Liu, F. Liu, *Nat. Commun.* **2013**, *4*, 2451.
- [105] Z. F. Wang, N. H. Su, F. Liu, *Nano Lett.* **2013**, *13*, 2842.
- [106] L. Z. Zhang, Z. F. Wang, B. Huang, B. Cui, Z. M. Wang, S. X. Du, H. J. Gao, F. Liu, *Nano Lett.* **2016**, *16*, 2072.
- [107] L. Dong, Y. Kim, D. Er, A. M. Rappe, V. B. Shenoy, *Phys. Rev. Lett.* **2016**, *116*, 096601.
- [108] A. Kumar, K. Banerjee, A. S. Foster, P. Liljeroth, *Nano Lett.* **2018**, *18*, 5596.
- [109] T. Kambe, R. Sakamoto, K. Hoshiko, K. Takada, M. Miyachi, J. H. Ryu, S. Sasaki, J. Kim, K. Nakazato, M. Takata, H. Nishihara, *J. Am. Chem. Soc.* **2013**, *135*, 2462.
- [110] M. Zhou, W. M. Ming, Z. Liu, Z. F. Wang, P. Li, F. Liu, *Proc. Natl. Acad. Sci. USA* **2014**, *111*, 14378.

- [111] C. H. Hsu, Z. Q. Huang, F. C. Chuang, C. C. Kuo, Y. T. Liu, H. Lin, A. Bansil, *New J. Phys.* **2015**, *17*, 025005.
- [112] Z. F. Wang, K. H. Jin, F. Liu, *Nat. Commun.* **2016**, *7*, 12746.
- [113] N. N. Hao, J. P. Hu, *Phys. Rev. X* **2014**, *4*, 031053.
- [114] Y. H. Yuan, W. Li, B. Liu, P. Deng, Z. L. Xu, X. Chen, C. L. Song, L. L. Wang, K. He, G. Xu, X. C. Ma, Q. K. Xue, *Nano Lett.* **2018**, *18*, 7176.
- [115] J. F. Ge, Z. L. Liu, C. H. Liu, C. L. Gao, D. Qian, Q. K. Xue, Y. Liu, J. F. Jia, *Nat. Mater.* **2015**, *14*, 285.
- [116] Q. Y. Wang, Z. Li, W. H. Zhang, Z. C. Zhang, J. S. Zhang, W. Li, H. Ding, Y. B. Ou, P. Deng, K. Chang, J. Wen, C. L. Song, K. He, J. F. Jia, S. H. Ji, Y. Y. Wang, L. L. Wang, X. Chen, X. C. Ma, Q. K. Xue, *Chinese Phys. Lett.* **2012**, *29*, 037402.
- [117] Z. F. Wang, Z. Liu, J. L. Yang, F. Liu, *Phys. Rev. Lett.* **2018**, *120*, 156406.
- [118] S. Murakami, *Phys. Rev. Lett.* **2006**, *97*, 236805.
- [119] Z. Liu, C.-X. Liu, Y.-S. Wu, W.-H. Duan, F. Liu, J. Wu, *Phys. Rev. Lett.* **2011**, *107*, 136805.
- [120] A. Shitade, H. Katsura, J. Kunes, X. L. Qi, S. C. Zhang, N. Nagaosa, *Phys. Rev. Lett.* **2009**, *102*, 256403.
- [121] R. W. Zhang, C. W. Zhang, W. X. Ji, P. Li, P. J. Wang, S. S. Li, S. S. Yan, *Appl. Phys. Lett.* **2016**, *109*, 182109.
- [122] Z. J. Wang, H. M. Weng, Q. S. Wu, X. Dai, Z. Fang, *Phys. Rev. B* **2013**, *88*, 125427.
- [123] C. W. Niu, P. M. Buhl, G. Bihlmayer, D. Wortmann, Y. Dai, S. Blugel, Y. Mokrousov, *Phys. Rev. B* **2017**, *95*, 075404.
- [124] A. C. Ferrari, J. C. Meyer, V. Scardaci, C. Casiraghi, M. Lazzeri, F. Mauri, S. Piscanec, D. Jiang, K. S. Novoselov, S. Roth, A. K. Geim, *Phys. Rev. Lett.* **2006**, *97*, 187401.
- [125] J. H. Chen, C. Jang, S. D. Xiao, M. Ishigami, M. S. Fuhrer, *Nat. Nanotechnol.* **2008**, *3*, 206.
- [126] J. H. Chen, L. Li, W. G. Cullen, E. D. Williams, M. S. Fuhrer, *Nat. Phys.* **2011**, *7*, 535.
- [127] E. McCann, V. I. Fal'ko, *Phys. Rev. Lett.* **2012**, *108*, 166606.
- [128] S. Lara-Avila, S. Kubatkin, O. Kashuba, J. A. Folk, S. Luscher, R. Yakimova, T. J. B. M. Janssen, A. Tzalenchuk, V. Fal'ko, *Phys. Rev. Lett.* **2015**, *115*, 106602.
- [129] Y. Y. Yang, Z. Xu, L. Sheng, B. G. Wang, D. Y. Xing, D. N. Sheng, *Phys. Rev. Lett.* **2011**, *107*, 066602.
- [130] C. Weeks, J. Hu, J. Alicea, M. Franz, R. Q. Wu, *Phys. Rev. X* **2011**, *1*, 021001.
- [131] A. Cresti, V. D. Tuan, D. Soriano, A. W. Cummings, S. Roche, *Phys. Rev. Lett.* **2014**, *113*, 246603.
- [132] J. Hu, J. Alicea, R. Q. Wu, M. Franz, *Phys. Rev. Lett.* **2012**, *109*, 266801.
- [133] G. Autes, O. V. Yazyev, *Phys. Rev. B* **2013**, *87*, 241404.
- [134] Z. Z. Jia, B. M. Yan, J. J. Niu, Q. Han, R. Zhu, D. P. Yu, X. S. Wu, *Phys. Rev. B* **2015**, *91*, 085411.
- [135] U. Chandni, E. A. Henriksen, J. P. Eisenstein, *Phys. Rev. B* **2015**, *91*, 245402.
- [136] Y. L. Wang, S. D. Xiao, X. H. Cai, W. Z. Bao, J. Reutt-Robey, M. S. Fuhrer, *Sci. Rep.* **2015**, *5*, 15764.
- [137] J.-H. C. Chao-Yi Cai, *Chinese Phys. B* **2018**, *27*, 67304.
- [138] B. A. Barker, A. J. Bradley, M. M. Ugeda, S. Coh, A. Zettl, M. F. Crommie, S. G. Louie, M. L. Cohen, *Phys. Rev. B* **2019**, *99*, 075431.
- [139] K. Hatsuda, H. Mine, T. Nakamura, J. Li, R. Wu, J. Alicea, S. Katsumoto, J. Haruyama, *Sci. Adv.* **2018**, *4*, eaau6915.
- [140] T. Namba, K. Tamura, K. Hatsuda, T. Nakamura, C. Ohata, S. Katsumoto, J. Haruyama, *Appl. Phys. Lett.* **2018**, *113*, 053106.
- [141] Z. Wang, D. K. Ki, H. Chen, H. Berger, A. H. MacDonald, A. F. Morpurgo, *Nat. Commun.* **2015**, *6*, 8399.
- [142] J. H. Garcia, A. W. Cummings, S. Roche, *Nano Lett.* **2017**, *17*, 5078.
- [143] B. W. Yang, M. F. Tu, J. Kim, Y. Wu, H. Wang, J. Alicea, R. Q. Wu, M. Bockrath, J. Shi, *2D Mater.* **2016**, *3*, 031012.
- [144] A. W. Cummings, J. H. Garcia, J. Fabian, S. Roche, *Phys. Rev. Lett.* **2017**, *119*, 206601.
- [145] G. W. Burg, N. Prasad, K. Kim, T. Taniguchi, K. Watanabe, A. H. MacDonald, L. F. Register, E. Tutuc, *Phys. Rev. Lett.* **2018**, *120*, 177702.
- [146] K. S. Novoselov, Z. Jiang, Y. Zhang, S. V. Morozov, H. L. Stormer, U. Zeitler, J. C. Maan, G. S. Boebinger, P. Kim, A. K. Geim, *Science* **2007**, *315*, 1379.
- [147] Q. F. Sun, X. C. Xie, *Phys. Rev. Lett.* **2010**, *104*, 066805.
- [148] A. F. Young, C. R. Dean, L. Wang, H. Ren, P. Cadden-Zimansky, K. Watanabe, T. Taniguchi, J. Hone, K. L. Shepard, P. Kim, *Nat. Phys.* **2012**, *8*, 550.
- [149] J. D. Sanchez-Yamagishi, J. Y. Luo, A. F. Young, B. M. Hunt, K. Watanabe, T. Taniguchi, R. C. Ashoori, P. Jarillo-Herrero, *Nat. Nanotechnol.* **2017**, *12*, 118.
- [150] J. P. Eisenstein, A. H. MacDonald, *Nature* **2004**, *432*, 691.
- [151] J. I. A. Li, T. Taniguchi, K. Watanabe, J. Hone, C. R. Dean, *Nat. Phys.* **2017**, *13*, 751.
- [152] X. M. Liu, K. Watanabe, T. Taniguchi, B. I. Halperin, P. Kim, *Nat. Phys.* **2017**, *13*, 746.
- [153] K. Lee, J. Xue, D. C. Dillen, K. Watanabe, T. Taniguchi, E. Tutuc, *Phys. Rev. Lett.* **2016**, *117*, 046803.